NUMERICAL ANALYSIS OF TURBULENT GAS-SOLID FLOWS IN A ROUGH HORIZONTAL CHANNEL USING THE EULERIAN TWO-FLUID MODEL

A Thesis

submitted to the College of Graduate and Postdoctoral Studies

in Partial Fulfillment of the Requirements for the Degree of

Master of Science

In the Department of Mechanical Engineering

University of Saskatchewan

Saskatoon, Saskatchewan, Canada

By

Anurag Das

PERMISSION TO USE

In presenting this thesis in partial fulfillment of the requirements for a Postgraduate degree from the University of Saskatchewan, I agree that the Libraries of this University may make it freely available for inspection. I further agree that permission for copying of this thesis in any manner, in whole or in part, for scholarly purposes may be granted by the professor or professors who supervised my thesis/dissertation work or, in their absence, by the Head of the Department or the Dean of the College in which my thesis work was done.

It is understood that any copying or publication or use of this thesis or parts thereof for financial gain shall not be allowed without my written permission. It is also understood that due recognition shall be given to me and to the University of Saskatchewan in any scholarly use which may be made of any material in my thesis.

Requests for permission to copy or to make other uses of materials in this thesis in whole or part should be addressed to:

Head of the Department of Mechanical Engineering
University of Saskatchewan
Engineering Building, 57 Campus Drive
Saskatoon, SK S7N 5A9
Canada

OR

Dean
College of Graduate and Postdoctoral Studies
University of Saskatchewan
116 Thorvaldson Building, 110 Science Place
Saskatoon, SK S7N 5C9
Canada

ABSTRACT

Turbulent gas-solid flows are encountered in many industrial processes including pneumatic transport of granular materials such as pulverized coal, circulating fluidized beds and dust and particle-exhaust pollution control systems. Modelling the gas-solid flow is a major challenge since the flow is turbulent which renders the system non-linear. In addition, the presence of particles further complicates the flow. The two-fluid formulation is a popular approach for modelling gas-particle flows that describes the motion of both phases in an Eulerian framework.

The current dissertation explores the effects of wall roughness on the particle-phase properties of a turbulent gas-solid flow in a horizontal channel. An in-house numerical code is modified to simulate a fully developed turbulent gas-solid flow; the numerical code is based on the two-fluid formulation adopted from the model of Rao et al. (2011). The gas-solid flow in the horizontal channel is asymmetric due to the gravity acting transverse to the flow. Three different studies were conducted to document the response of the particle-phase properties to different flow conditions.

The first study focuses on the effect of hydrodynamic roughness on the gas-solid flow. The hydrodynamic effect of wall roughness was implemented in the model using a two-layer version of the k - ε model based on Durbin et al. (2001). The thesis documents outcomes of the simulations that compare the flow for the rough wall with that for the smooth wall. It was found that the hydrodynamic roughness energized the particles present in the flow via turbulence modulation.

Wall roughness alters the particle-wall interactions. The particle-wall interactions were characterized using the boundary conditions of Johnson and Jackson (1987), which defined the specularity coefficient. The second study focuses specifically on the role of the specularity coefficient in characterizing wall roughness. The channel wall is rough from a particle perspective. The outcomes of the simulations were compared to the experimental study of Sommerfeld and Kussin (2004). The experiment explores the effect of different levels of wall roughness on the particle-phase properties.

The dissertation documents the comparisons between the simulations and the experimental data for the mean solids velocity and the solids volume fraction profiles. The profiles for properties like turbulence kinetic energy, granular temperature, solids viscosity and solids shear stress for different levels of roughness were also documented and analyzed. It was found that specularity

coefficient plays a significant role in characterizing the wall roughness. The predicted profiles for the mean solids velocity and the solids volume fraction deviated from the experimental profile in the near-wall region. The degree of deviation from the experimental data decreased with an increase in the specularity coefficient. This implies that the specularity coefficient is less effective for walls with smaller roughness.

The third study focuses on the sensitivity of the particle-phase properties to three different parameters; the specularity coefficient, the mass loading and the Stokes number. Increasing the specularity coefficient increases the number of diffuse particle-wall collisions. It was found that increasing specularity coefficient increased the granular temperature, which resulted in higher predictions for the solids viscosity and the solids shear stress. The increase in the mass loading increased the number of particles present in the flow. It was found that the increase in mass loading increased the granular temperature by increasing the frequency of particle-wall collisions. The effect of particle inertia was investigated by increasing the Stokes number. The solids velocity monotonically decreases with an increase in the Stokes number while the behaviour of the granular temperature and solids shear stress were more complicated.

ACKNOWLEDGEMENTS

I would like to thank Prof. Donald J. Bergstrom, my research supervisor from the bottom of my heart, for guiding, supporting and motivating me through the Master's program. His critique of my research and helpful suggestions, helped me achieve the end goals of my research.

I would like to express my gratitude towards my advisory committee members, Prof Jim Bugg, Prof Scott Noble, and Dr. Ryan Spelay, for their invaluable feedback and suggestions.

I would like to take the time to thank A.S.M. Atiqul Islam, Md. Reza Haghgoo, Rajat Chakravarty, for their guidance, and advice on important topics essential to both my academic as well as my research endeavors at the University of Saskatchewan.

I would like to thank Ming Teng, Bhaskar Paliwal, Hadi Hosseinzade, and other friends at the CFD Lab as well as in the Department of Mechanical Engineering for their kind help and support. I would also like to thank Shawn Reinink for his invaluable help.

I would once again like to thank Prof. Bergstrom, CGSR, and NSERC for providing the financial support for this research work.

DEDICATED TO

My Parents and my sister, for their unconditional support, and words of motivation.

TABLE OF CONTENTS

LIST OF FIGURES

LIST OF TABLES

LIST OF SYMBOLS

d_p	Particle diameter (μm)
e	Particle coefficient of restitution
E_w	Wake effect ($\mathrm{kg \cdot m^{-1} \cdot s^{-3}}$)
e_w	Particle-wall coefficient of restitution
g_o	Particle distribution function
I_K	Fluid-phase turbulence modulation term ($\mathrm{kg \cdot m^{-1} \cdot s^{-3}}$)
I_T	Solid-phase turbulence modulation term ($\mathrm{kg \cdot m^{-1} \cdot s^{-3}}$)
k	Turbulence kinetic energy ($\mathrm{m^2 \cdot s^{-2}}$)
k_{sf}	Cross-correlation term for fluctuating velocities ($\mathrm{m^2 \cdot s^{-2}}$)
m	Mass loading
P	Pressure (Pa)
q_{PT}	Pseudo-thermal energy flux vector ($\mathrm{kg \cdot s^{-3}}$)
r^+	Non-dimensionalized roughness height; $\left(= \frac{ru_\tau}{\nu}\right)$
Re_s	Particle Reynolds number
Re	Reynolds number of the flow
St	Stokes number of the flow
T	Granular temperature ($\mathrm{m^2 \cdot s^{-2}}$)
u_f	Mean fluid-phase velocity in the stream-wise direction ($\mathrm{m \cdot s^{-1}}$)

u_s	Mean solid-phase velocity in the stream-wise direction ($m \cdot s^{-1}$)
$u_f^{'}$	Fluctuating velocity in the gas-phase ($m \cdot s^{-1}$)
$u_s^{'}$	Fluctuating velocity in the solid-phase ($m \cdot s^{-1}$)
u_τ	Wall-friction velocity ($m \cdot s^{-1}$)
x	Stream-wise coordinate (m)
y	Wall-normal coordinate (m)
y_{eff}	Effective wall-normal distance (m)
y_0	Average roughness height (m)

Greek Symbols

α_o	Maximum packing fraction
α_f	Fluid-phase volume fraction
α_s	Solid-phase volume fraction
β	Drag coefficient ($kg \cdot m^{-1} \cdot s^{-3}$)
γ	Granular dissipation ($kg \cdot m^{-1} \cdot s^{-3}$)
ε	Dissipation of turbulence kinetic energy ($m^2 \cdot s^{-3}$)
λ_p	Mean free path of the particles (m)
μ_{ef}	Effective gas-phase eddy viscosity ($kg \cdot m^{-1} \cdot s^{-1}$)
μ_f	Viscosity of gas-phase ($kg \cdot m^{-1} \cdot s^{-1}$)

μ_s	Viscosity of solid-phase ($kg \cdot m^{-1} \cdot s^{-1}$)
μ_t	Turbulent viscosity of gas-phase ($kg \cdot m^{-1} \cdot s^{-1}$)
v_f	Kinematic viscosity for the gas-phase ($m^2 \cdot s$)
v_s	Kinematic viscosity for the solid-phase ($m^2 \cdot s$)
ρ_f	Gas-phase density ($kg \cdot m^{-3}$)
ρ_s	Solid-phase density ($kg \cdot m^{-3}$)
σ_{xy}	Solid-phase shear stress (Pa)
σ_{yy}	Solid-phase normal stress (Pa)
τ_C	Collsional time-scale (s)
τ_D	Drag time-scale (s)
τ_{sf}	Fluctuating energy transfer time-scale (s)
τ_{xy}	Gas-phase shear stress (Pa)
ϕ	Specularity coefficient
ω	Damping function for the solid-phase

Subscripts

f	Indicates the fluid/gas phase
$\boldsymbol{s}$	Indicates the solid-phase

Superscripts

$'$	Indicates the fluctuating component of the variable
$+$	Indicates the non-dimensionalized quantity using the wall-friction velocity

CHAPTER 1: INTRODUCTION

Computational Fluid Dynamics (CFD) is widely used to simulate and visualize complex flows, which are inherently difficult and costly to investigate through experimental studies. Most CFD simulation techniques are based on the Navier - Stokes equations, which define the motion of a Newtonian fluid. However, if another immiscible liquid or a discrete solid is present in the same flow, the dynamics of the flow will change. The behavior of the fluid remains true to the Navier – Stokes equations, but there is also an additional variable in the system, i.e. the motion of the other phase, whose behavior and contribution to the fluid flow is unknown. The research presented in this thesis explores and expands on this theme.

1.1 TWO-PHASE FLOW

Two-phase flow refers to a system consisting of two different phases, such as gas and liquid, gas and solid, or liquid and solid flowing together as a mixture. The two phases interact with each other and usually have different velocities. The main focus of this research will be on turbulent gas-solid flows. Turbulent gas-solid flows are encountered in numerous industrial processes including pneumatic transport of granular materials such as coal, circulating fluidized beds, and dust and particle-exhaust pollutant control systems. Modelling gas-solid flow is a major challenge when the flow is turbulent which renders the system non-linear; the presence of particles further complicates the flow.

Modeling gas-solid flows is an active research topic and there is not yet a single comprehensive model that accurately predicts the behavior of all turbulent gas-solid flows. If the constituents of the two-phase flow are indistinguishable, then mixture models can be used to describe the flow. These include:

1) Homogenous model: Owen *et al.* (1976) describe a model in which the two-phase flow is treated as a single-phase flow having pseudo-properties calculated by suitably weighting the properties of the individual phases;

2) Drift flux model: The drift flux model also considers the mixture as a whole rather than the two phases separately. As per Ishii and Hibiki (2006) this model is based on the mixture continuity, and momentum equations, plus the continuity equation of the other phases. The mixture properties such as density and viscosity are obtained by Favre averaging based on the proportions of each phase present in the flow.

If the properties of the components of a two-phase flow are distinct from each other, then the following approaches can be used:

1) Eulerian-Lagrangian approach: In this approach each of the particles is considered individually. The model tracks the dynamics of every particle in the flow;
2) Eulerian-Eulerian approach: In this approach, often referred to as the two-fluid model, both the fluid phase and the solid phase are considered as inter-penetrating continua. This model formulation predicts the time-averaged motion of both phases.

The main advantage of the two-fluid model is that it predicts the solid phase behaviour without tracking particles individually. For this reason that the two-fluid modelling approach has been adopted for the research presented in this thesis.

1.2 LITERATURE REVIEW

1.2.1 General

One of initial attempts to model a turbulent gas-solid flow was by Tchen (1947), which explored the motion of particles in a turbulent fluid flow. However, the work only explored motion of a single particle, analyzing the time-averaged flow parameters. This initial attempt represented an Eulerian-Lagrangian approach to solving the problem. The Eulerian-Lagrangian approach can be used as long as there are a limited number of particles in a flow; however, when there are many particles, it is inefficient to track each of them to define the characteristics of the overall flow. Instead, the particle phase can be modelled as a continuum. Anderson and Jackson (1967), instead of defining the local point variables for the particle and the fluid phases, used volume-averaged values for each phase. The particle-phase was treated as a continuum and both phases were assumed to co-exist at all points, as defined by the volume fraction. Thus originated the approach known today as the two-fluid model (TFM). The solids volume fraction is the ratio of the volume of the particles to the total volume of the flow. Based on the solids volume fraction and the Stokes number, Elgobashi (1994) classified gas-solid flows into three different regimes. Stokes number

is a ratio of the particle relaxation time to a relevant fluid time scale. The particle relaxation time represents the time taken by the particle to respond to the fluid phase velocity, and is dependent on the density and diameter of the particle. The Stokes number is in general indicative of the particle inertia. The three different regimes identified by Elgobashi (1994) are:

1) One-way coupling: When particles have negligible effect on the gas-phase dynamics, this is known as one-way coupling. According to Zhang and Reese (2003) the solids volume fraction must be less than 10^{-6} for the particles to have little or no effect on the gas-phase dynamics.
2) Two-way coupling: When the solids volume fraction is greater than 10^{-6}, the particles will either enhance or suppress gas-phase turbulence depending on the Stokes number. Periano and Leckner (1998) explain that, when the Stokes number is greater than 10^{2}, particles enhance turbulence through vortex shedding. When Stokes number is below 10^{2}, there is no vortex shedding and the energy is extracted from eddies to accelerate the particles present. Hence, a suppression in gas-phase turbulence is observed. This is called two-way coupling.
3) Four-way coupling: When collisions begin to play an important role, in addition to the particle-fluid and fluid-particle interactions, a four-way coupling is observed. Due to the non-linear nature of these interactions, the effect of Stokes number in this regime is complex.

There are numerous mathematical models to simulate gas-solid flows using the two-fluid approach. Rao *et al*. (2011) suggest that the models primarily vary based on the following aspects:

1) The drag model;
2) The particle stress model;
3) Turbulence modulation term.

The following subsections discuss the above-mentioned aspects of the two-fluid model.

1.2.1.1 Drag models

The drag term is the dominant interfacial force that couples the transport equations of the mean velocities of both phases. Bolio *et al.* (1995) used the drag coefficient formulation proposed by Ding and Gidaspow (1990). Hadinoto and Curtis (2009) showed that the choice of drag model affects the predicted mean and fluctuating velocity profiles in dilute gas-solid flow for small and low density particles at low velocities. Rao *et al.* (2011) tested the drag models of Wen and Yu (1966), Hill *et al*. (2001a, 2001b), as well as the model of Benyahia *et al.* (2007); the drag models differed from each other in terms of the mathematical constant used to empirically fit the

experimental data. They found that the drag model of Hill *et al*. (2001a, 2001b) tended to under-predict the drag force due to the particles which the model of Benyahia *et al.* (2007) tended to over-predict the drag force due to the particles, while the model by Wen and Yu (1966) gave the best agreement to experimental data.

1.2.1.2 Particle stress models

The particle stresses are generated by direct particle-particle interactions and particle-wall interactions. Zhang and Reese (2003) identified two approaches for modelling particle stresses: empirical models and the kinetic theory of granular flow. The empirical models are developed from experimental data. The kinetic theory of granular flow is more rigorous, but is often criticized as unsuitable because of the differences between a dry granular system and a gas-particle two-phase system. In a gas-particle flow, the particles are subject to forces due to the gas phase. However, the influence of gas-phase forces on the particulate phase is ignored in the kinetic theory of dry granular flow.

Savage and Jeffrey (1981) compared the random motion of particles to that of gas molecules and borrowed the ideas of the kinetic theory of gases to model granular flow. Sinclair and Jackson (1989) used the kinetic theory of gas-solid flow to model the particle stresses, which is the most commonly adopted model.

Lun *et al.* (1984) captured the macroscopic behavior of the solid phase by solving the velocity distribution function using the Boltzmann equation. The particle-particle collisions were modelled using the binary collision theory of inelastic hard spheres. The velocity fluctuation of the solid-phase is described using the concept of granular temperature. A second-order moment equation was used to model the transport equation of the granular temperature which is analogous to the turbulence kinetic energy equation. Bolio *et al.* (1995) adopted this model to describe the stresses developed in the solid-phase.

The interstitial fluid effects are often neglected in a kinetic theory model by assuming that the random motion of particles is controlled by inter-particle collisions. However, this assumption is only valid when the particle relaxation time is larger than the particle collision time (time between consecutive particle collisions). In relatively dilute flows with small Stokes numbers, the motion of the particles will be affected by both the gas-turbulent fluctuations and the mean flow. In this

case interstitial effects are present. Peirano and Leckner (1998) showed that interstitial fluid effects can be neglected in the case of a very dilute gas-particle flow for large Stokes numbers, since the particle motion is not affected by the gas-phase velocity due to the high inertia of the particle. The stress model by Peirano and Leckner (1998), which was employed by Zhang and Reese (2003), includes the effects of the interstitial fluid. Rao *et al.* (2011) compared the particle stress model of Lun *et al.* (1984) to the particle stress model of Periano and Leckner (1998), and concluded that the model of Peirano and Leckner (1998) is better suited to dilute, turbulent gas-solid flows.

1.2.1.3 Turbulence modulation

Although many studies include turbulence modulation, there is no comprehensive model for the effect. Direct numerical simulation (DNS) has been the preferred method for studying turbulence modulation. Zhang and Reese (2003) suggest that particle size, density and volume fraction are that factors that affect turbulence modulation. Gore and Crowe (1989), on the basis of their experimental data, proposed that larger particles (ratio of particle diameter d to turbulent length scale l, $d/l > 0.1$) tend to augment the turbulence, while smaller particles ($d/l \leq 0.1$) tend to suppress it. The paper by Crowe (1997) indicates that turbulence modulation may be due to the wakes of particles, the deformation of the flow field by particles, turbulent energy transfer and the modification of velocity gradients.

Time and volume based averaging is used to develop expressions for the turbulence modulation. Louge *et al.* (1991) formulated the fluctuating term based on the gas-phase turbulence, granular temperature and the gas-solid velocity cross correlation. Yuan and Michaelides (1992) argued that the particle wake contributes to the augmentation of the gas-phase turbulence and the work done on the particles is responsible for the suppression of turbulence. Bolio *et al.* (1995) used time and volume based averaging, and modified the model of Koch (1990) using a cross-correlation term based on the particle-phase inertia and viscous forces of the fluid-phase. Bolio *et al.* (1995) assumed that the inertia of the fluid is minimal and that the particle interactions occur at small particle Reynolds numbers. They noted that this method could not predict turbulence augmentation and the gas-phase turbulence was under-predicted.

Bolio and Sinclair (1995) predicted the turbulence augmentation for large 500 μm particles, but failed to reproduce the observed augmentation for the smaller 200 μm particles at higher mass loading. Crowe (2000) indicated that derivations which assumed the averaged properties of the

flow to be local flow properties are inconsistent. He argued that an approach to the derivation of the turbulence kinetic energy transport equation, which treats the averaged velocity as a local velocity in the momentum equation of both phases, is inappropriate. Rather one should derive the turbulence kinetic energy equations from the instantaneous Navier-Stokes equation. However Zhang and Reese (2003) found limited agreement with the experimental data using the turbulence model suggested by Crowe (2000) in their closure model.

Rao *et al.* (2011) modelled the fluctuating energy transfer terms on the basis of a convection heat transfer analogy. They modelled the gas-phase velocity fluctuations as the sole source-term of the particle-phase velocity fluctuations. The model for the cross-correlation term proposed by Sinclair and Mallo (1998) was used by Rao *et al.* (2011) for the gas-solid fluctuating velocity cross-correlation. Sinclair and Mallo (1998) specified the gas-solid fluctuating velocity cross-correlation in terms of the solid-phase granular temperature and the gas-phase turbulence kinetic energy. These formulations account for particle-wall collisions and allow for particle slip at the wall, giving rise to a change in sign of the relative mean velocity between the phases near the wall.

1.2.2 Boundary conditions and the effect of wall roughness

Bolio *et al.* (1995) used a no-slip boundary condition for a smooth wall, which is a commonly used boundary condition in the low Reynolds number $k - \varepsilon$ model for the fluid-phase. Rao *et al.* (2011) applied two different boundary conditions: the no-slip boundary condition as per Bolio *et al.* (1995), and wall functions.

There also have been numerous attempts to include the effect of wall roughness in two-fluid models. Wall roughness affects both the particle phase and the fluid phase. For the fluid phase, the flow becomes hydrodynamically rough in the near-wall region. A limitation in the high Reynolds number $k - \varepsilon$ model is its inability to describe the near-wall region, which in turn makes it difficult to include the effects of surface roughness. To include the effects of surface roughness, Fan and Ahmadi (1993) included a sublayer model and altered the particle phase boundary conditions for deposition of particles in vertical ducts. The results were in agreement with the experimental data. The sublayer model was later used for simulating aerosol transport and deposition in a horizontal channel by Li and Ahmadi (2000) and Zhang and Ahmadi (2000). Zaman and Bergstrom (2014) adopted the two-layer model by Durbin *et al.* (2001), which incorporates the effect of surface

roughness on the fluid-phase by introducing an equivalent hydrodynamic roughness length into the inner layer.

The solid-phase boundary conditions are based on the proposals of the seminal work of Johnson and Jackson (1987). They classify the particle interactions at the wall in a gas-solid flow as either a long contact or a short contact. The longer contacts are assumed to be frictional contacts either between particles or between a particle and the wall, and involve significant points of momentum transfer; the shorter contacts are collisional contacts. The longer contacts are diffuse in nature; the shorter contacts are specular in nature. The nature of particle interactions at the wall is modelled based on an analogy to the laws defining the reflection of light. Giancoli (1984) discusses that a smooth surface will create a specular reflection when light rays are incident onto it; a rough surface will create a diffuse reflection. The "diffuseness" of the reflection is a complicated variable of the topology of a rough surface. Similarly as per Johnson and Jackson (1987), a smooth surface will have specular collisions while a rough surface will have diffuse collisions. They define the specularity coefficient as the ratio of the diffuse collisions to the total number of collisions at the wall. A specularity coefficient of 0 indicates a perfectly smooth wall, while a specularity coefficient of 1 indicates a rough wall with only diffuse particle interactions at the wall. Diffuse collisions are indicative of the surface roughness, hence by setting the specularity coefficient to a certain finite value below 1, surface roughness is characterized. The solids shear stress at the wall, and the energy flux at the wall were determined on the basis of the specularity coefficient used.

There are other advanced models that introduce the effects of roughness on the particle-phase through the boundary conditions for the wall solid stress and the wall energy flux. Schneiderbauer *et al.* (2012) uses the model of Louge *et al.* (1991) to describe boundary conditions for a smooth wall. They define the production and dissipation of the particle pseudo-thermal energy by using the particle-wall coefficient of restitution and the wall friction coefficient to account for the specular and diffuse particle-wall collisions, respectively. Soleimani *et al*. (2015) further developed the model by including the concept of virtual-wall angle to introduce the effect of roughness on the particle-phase. Virtual-wall angle is a concept introduced by Sommerfeld (1992), where the wall is assumed to be inclined at an angle which is proportional to the wall roughness. The model of Soleimani *et al.* (2015) was found to agree with experimental data for lower levels

of roughness, but failed to achieve agreement with experimental data for higher levels of roughness.

1.2.3 Experimental studies

The literature presents a limited number of experimental data sets for turbulent gas-solid flows in a rough horizontal channel. Laser Doppler Anemometry (LDA) is a popular non-intrusive method for measuring gas-solid flows as conceived by Yeh and Cummins (1964). The measuring "probe" is a fringe-pattern created by the interference of two coherent laser beams and is referred to as the measuring volume. Particles change the fringe pattern and reflect the light. The reflection is collected by a photodiode and is turned into a Doppler-burst signal recorded by the instrument.

Kussin and Sommerfeld (2002) studied the effects of channel wall roughness on particle conveyance and turbulence modulation. The roughness of the channel was varied, and the effect on the mean velocities of both the phases was explored. Sommerfeld and Kussin (2004) conducted a similar study to explore the contribution of wall roughness to the pressure loss in pneumatic conveyance. The roughness of the channel was varied similar to that of Kussin and Sommerfeld (2002) and the effects of particle size and its interaction with that of a rough-wall was explored. Cao and Ahmadi (2000) conducted a study of dilute gas-solid turbulent flow in a rough horizontal duct. Key flow properties were explored along with the effect of particle size on the flow. However, the study does not clearly quantify the wall roughness used.

1.2.4 Previous Research

Research by previous graduate students in this group have dealt with the numerical analysis of gas-solid flows in a smooth vertical pipe, e.g. Yerrumshetty (2007). Zaman (2013) considered a numerical analysis of gas-solid flows in a vertical pipe with rough walls, and also explored the turbulence modulation term proposed by Rao *et al.* (2011).

1.3 OBJECTIVES

The overall objective of the current study is to perform a numerical analysis of fully developed gas-solid flow in a horizontal channel using a two-fluid model formulation together with a two-layer wall turbulence model. The effect of a rough wall on the particle transport will be considered.

The specific objectives of the research are:

1) To modify an in-house numerical code to predict a fully-developed turbulent gas-solid flow in a horizontal channel that is asymmetric due to the effect of gravity on the particles present in the flow. The effect of smooth and rough hydrodynamics on the flow will be compared.
2) To implement the boundary condition proposed by Johnson and Jackson (1987) and assess its ability to express the effects of roughness on the particle phase in a channel with minimal roughness. The model performance will be assessed by comparing the predictions for the rough wall case with experimental data from literature, i.e. Sommerfeld and Kussin (2004), and Kussin and Sommerfeld (2002).
3) To conduct a parametric study of the effects of varying the specularity coefficient, mass loading of the particles present in the flow, and the particle Stokes number on the particle-phase parameters.

1.4 METHODOLOGY

An outline of the research program is given in Figure 1.1. The first step towards the development of a mathematical model that can predict gas-particle interactions will be to understand the underlying flow physics. The mathematical model is based on the two-fluid approach which assumes both the phases to be inter-penetrating continua. The phasic transport equations are modelled based on the model by Bolio et al. (1995). The fluid-phase turbulence is modelled as per the two-layer model proposed by Durbin et al. (2001), which introduces the effects of hydrodynamic roughness on the fluid-phase.

The current research deals with gas-solid flows with solids volume fraction ranging from 0.01% to 0.05%, however, a four-way coupling regime is implemented to demonstrate the effect of channel roughness on the flow.

The motion of the particles is modelled based on the model of Rao et al. (2011). The drag forces due to the particles is modelled based on the model of Wen and Yu (1966), which is the most reliable and widely used model. Based on the recommendation of Rao et al. (2011), the particle stress model of Peirano and Leckner (1998) is adopted for the mathematical model in the current code. The fluctuating phases interact with each other through the turbulence modulation term. The current study adopts the model of Sinclair and Mallo (1998) to account for the turbulence modulation interaction between the phases present in the flow.

For the current research, an in-house numerical code written in FORTRAN was preferred over commercial software. An in-house code provides the user with a higher degree of control compared to a commercial CFD software packages such as CFX and FLUENT. An in-house code also provides the user with the flexibility to readily implement new models and solution methods. However, this does not imply that commercial software packages are not useful. However, from the perspective of the current research, the advantages of using an in-house numerical code greatly outweigh those offered by a commercial software package.

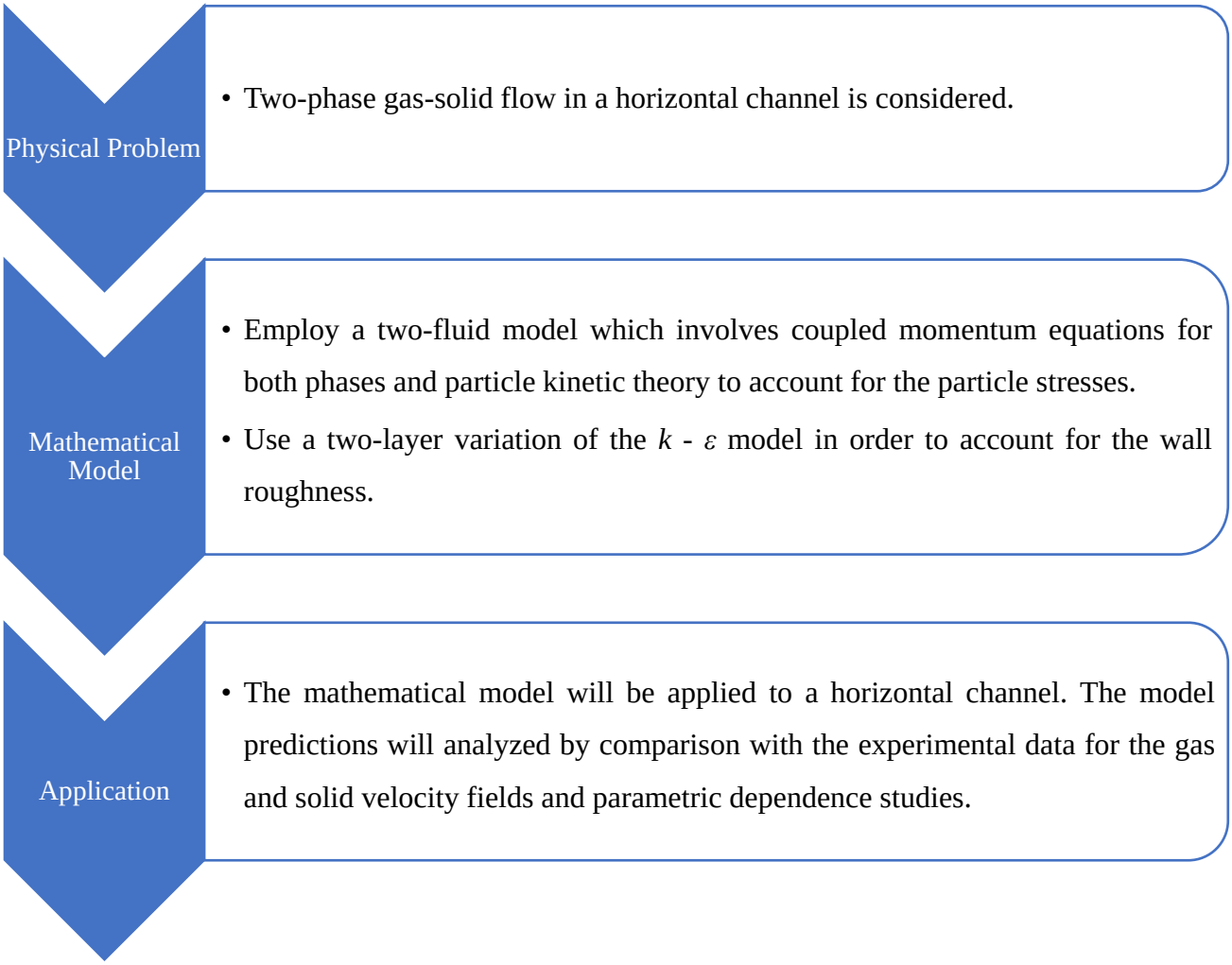

Figure 1.1: Overview of the methodology employed

1.5 THESIS STRUCTURE

The thesis has been structured in terms of four chapters. Chapter 1 consists of an introduction, a brief literature review and statement of the objectives. Chapter 2 describes the mathematical model employed for simulating the gas-solid flow in a horizontal channel. Chapter 3 documents the performance of the mathematical model using comparisons to experimental measurements. Chapter 4 documents the conclusions that can be drawn from the present work, and identifies some topics for further investigation.

CHAPTER 2: COMPUTATIONAL MODEL

The mathematical model described in this chapter has been developed specifically for gas-solid flows in a horizontal channel. The flow is assumed to be steady, incompressible, and fully developed. The transport equations for each phase are expressed in an Eulerian framework using the two-fluid formulation. The primary model describing the continuum equations for both phases has been adapted from the work of Bolio *et al.* (1995). The following sections describe the governing and the constitutive relations used in the present mathematical model. The numerical implementation of the mathematical model is also described.

2.1 Fluid-Phase Transport equations

Figure 2.1 depicts the flow configuration of a gas-solid flow in a horizontal channel of width *H*. The transport equations for the fluid phase for fully developed flow with x and y denoting the stream-wise and wall-normal directions, respectively, are given below. Since the flow is fully developed, from the continuity equation, the fluid-phase velocity in the transverse direction, v_f is 0.

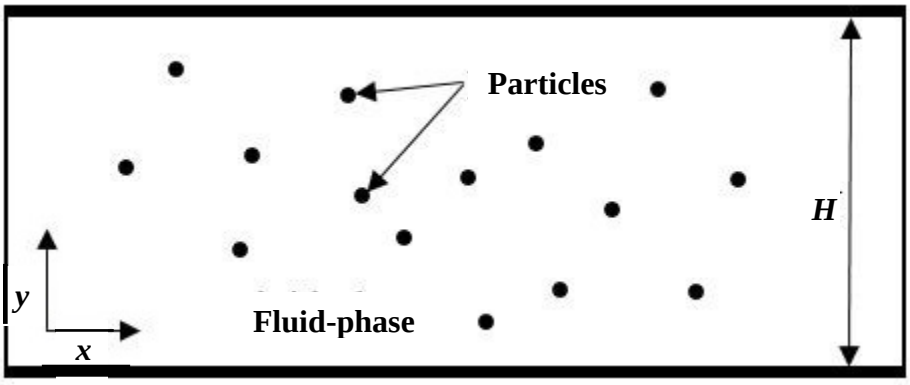

Figure 2.1: Flow configuration

The momentum transport in Equation (2.4) is based on the phase-averaged Navier-Stokes equation. Since the flow is fully developed, all the acceleration terms are zero. The resulting equation is given by:

$$0 = -\alpha_f \frac{\partial p}{\partial x} + \frac{\partial}{\partial y}\tau_{xy} - \beta\left(u_f - u_s\right) \tag{2.1}$$

where α_f is the fluid-phase volume fraction, $\partial p/\partial x$ is the fluid pressure gradient, τ_{xy} is the total shear stress, β is the interfacial drag term, u_f is the fluid-phase velocity in the stream-wise direction and u_s is the solid-phase velocity in the stream-wise direction. Since $v_f = 0$,the total shear stress, τ_{xy} is given by:

$$\tau_{xy} = \left(\mu_t + \mu_{ef}\right)\frac{\partial u_f}{\partial y} \tag{2.2}$$

where μ_t is the turbulent viscosity calculated in terms of the turbulence kinetic energy *k* and its dissipation ε by the relation

$$\mu_t = \frac{\rho_f c_\mu k^2}{\varepsilon} \tag{2.3}$$

In equation 2.3, c_μ is a model coefficient.

Batchelor and Green (1972) discuss that, in dilute flows, the particle phase and the fluid phase behave like a single fluid, whose viscosity is a function of the square of the solids volume fraction. They define an effective viscosity μ_{ef}, which is the given by

$$\mu_{ef} = \mu_f(1 + 2.5\alpha_s + 7.6\alpha_s^2)\left(1 - \frac{\alpha_s}{\alpha_0}\right) \tag{2.4}$$

Here, μ_f is the molecular viscosity, α_s is the solids volume fraction, α_0 is the maximum possible solids volume fraction at the packing limit.

The turbulence kinetic energy, used in the eddy viscosity model, is given by

$$k = \left(\frac{1}{2}\overline{u_f' u_f'} + \frac{1}{2}\overline{v_f' v_f'} + \frac{1}{2}\overline{w_f' w_f'}\right) \tag{2.5}$$

where a prime indicates the fluctuating fluid-phase velocity component, and ($\bar{}$) indicates time-averaging.

The dissipation rate of the turbulence kinetic energy, ε, represents the conversion of kinetic energy to thermal energy at the smallest scales of motion.

The interfacial drag term is the drag force that acts on the particles present in the flow, which also represents the effect of the particles on the carrier phase. The drag term formulation used here was originally proposed by Wen and Yu (1966), and is the most widely used model. It is given by

$$\beta = \frac{3}{4}\frac{\rho_f}{d} C_D \frac{\alpha_s}{\alpha_f^{2.65}} |u_f - u_s| \tag{2.6}$$

where the coefficient of drag C_D is given by

$$C_D = \frac{24}{Re_s}(1 + 0.15 Re_s^{0.687}) \tag{2.7}$$

where Re_s is the particle Reynolds number. It is based on the slip velocity, i.e.

$$Re_s = \frac{\rho_f d |u_s - u_f|}{\mu_f} \tag{2.8}$$

The values of k and ε are obtained from their respective transport equations. The mathematical model uses a two-layer modification for the $k - \varepsilon$ model. The model was originally proposed by Durbin *et al.* (2001) for single-phase flows. The two-layer formulation consists of a combination of two different models: a $k - \varepsilon$ model for the outer layer; a simplified k-based one equation model for the near-wall region called the inner layer.

For the outer layer, the transport equations are adopted from the single-phase $k - \varepsilon$ model developed by Jones and Launder (1972). The fluid phase volume fraction is incorporated into the equation to account for the phasic contribution of the fluid phase to the flow. The equations are given by

$$0 = \frac{\partial}{\partial y}\left\{\alpha_f \left(\mu_{ef} + \frac{\mu_t}{k}\right)\frac{\partial k}{\partial y}\right\} + \alpha_f \mu_t \left(\frac{\partial u_f}{\partial y}\right)^2 - \alpha_f \varepsilon - I_k \tag{2.9}$$

$$0 = \frac{\partial}{\partial y}\left\{\alpha_f \left(\mu_{ef} + \frac{\mu_t}{k}\right)\frac{\partial \varepsilon}{\partial y}\right\} + \alpha_f c_1 \frac{\varepsilon}{k}\mu_t \left(\frac{\partial u_f}{\partial y}\right)^2 - \alpha_f c_2 \frac{\varepsilon^2}{k} - \alpha_f c_3 \frac{\varepsilon}{k} I_k \tag{2.10}$$

To bring in the effect of the solid phase, a turbulence modulation term I_k is introduced into the transport equations above. The specific form of I_k is defined later. The model constants from

Durbin *et al.* (2001) are used for all the simulations in the study. They are: $c_1 = 1.4$, $c_2 = 1.8$, $c_3 = 1.2$, $\sigma_k = 1.4$, and $\sigma_\varepsilon = 1.3$.

For the inner layer, the turbulence kinetic energy is calculated using Equation (2.9), however, the dissipation is given by,

$$\varepsilon = \frac{k^{\frac{3}{2}}}{l_\varepsilon} \tag{2.11}$$

The eddy viscosity for the inner-layer is given by

$$\nu_t = C_\mu \sqrt{k} l_\nu \tag{2.12}$$

The VanDriest form for the length scales, l_ε and l_ν, respectively, are given by

$$l_\varepsilon = C_l y_{eff} \left(1 - e^{-\frac{R_y}{A_\varepsilon}}\right) \tag{2.13}$$

$$l_\nu = C_l y_{eff} \left(1 - e^{-\frac{R_y}{A_\nu}}\right) \tag{2.14}$$

where y_{eff} is the distance from the wall evaluated as

$$y_{eff} = y + y_o \tag{2.15}$$

Here y_o is the effective origin of the turbulence, which is added to the wall normal distance. The model constants for the near-wall region of the two-layer formulation are given by:

$$C_l = 2.5$$

$$A_\varepsilon = 2C_l = 5.0$$

and A_ν is a free constant. Durbin *et al.* (2001) empirically determined the value of the constant to be $A_\nu = A_\nu^0 = 62.5$ for the two-layer formulation. The R_y parameter is the wall distance Reynolds number given by, $R_y = \frac{y_{eff}\sqrt{k}}{\nu}$.

The two-layer formulation uses equations (2.9) and (2.10) for the outer layer and abruptly switches over to equations (2.11) and (2.12) for the inner layer at the patching point. The patching point is the location where the damping function $1 - \mathrm{e}^{-\frac{\mathrm{R_y}}{A_\nu^0}} = 0.95$.

Wall roughness disrupts the viscous sublayer. Conceptually, the effective origin y_o is a point where the mean fluid-phase velocity can be extrapolated to zero. The disruption in the viscous sublayer due to the wall roughness is accounted for by assigning a finite value to y_o. The finite value of y_o is based on the equivalent sand grain roughness of the rough wall, and the shift in the origin represents the hydrodynamic roughness. For a smooth wall, due to the absence of any dislocation of the viscous sublayer, y_o is set to zero.

2.2 Solid-Phase Transport Equations

The two-fluid formulation treats both the continuous phase and the discrete phase as continua. This means that the motion of the particles in the solid-phase is described in an Eulerian framework. The momentum transport equations for the solid-phase are given by

$$0 = \frac{\partial}{\partial y}\left(\frac{\partial \sigma_{xy}}{\partial y}\right) + \beta\left(u_f - u_s\right) \tag{2.16}$$

for the stream-wise (horizontal) direction, and

$$0 = \frac{\partial}{\partial y}\left(\sigma_{yy}\right) - \alpha_s \rho_s g \tag{2.17}$$

for the wall-normal (vertical) direction.

In the above equations, σ_{xy} is used to denote the particle shear stress and σ_{yy} is used to denote the particle normal stress. These expressions are components of the stress tensor obtained from kinetic theory, according to which the particle stresses are due to particle-particle and particle-wall collisions.

Equation (2.16) accounts for the effect of the particle drag in the stream-wise momentum transport. Equation (2.17) accounts for the body force due to the weight of the particles in the wall-normal momentum transport.

The closure equations for the shear stress and the normal stress terms in equations (2.16) and (2.17) have been adopted from Bolio *et al.* (1995), and are given by

$$\sigma_{xy} = -\mu_s(\omega g_1 + g_2)\frac{\partial u_s}{\partial y} \tag{2.18}$$

$$\sigma_{yy} = \rho_s(\omega \alpha_s + 4\eta \alpha_s^2 g_0)T \tag{2.19}$$

In equations (2.18) and (2.19), μ_s is the solid-phase viscosity, and T is the solid-phase granular temperature. Both these terms are obtained from kinetic theory. The solid-phase viscosity is given by

$$\mu_s = \frac{5\sqrt{\pi} d_p \rho_s \sqrt{T}}{96} \tag{2.20}$$

The solid-phase granular temperature accounts for the solid-phase velocity fluctuations, and is given by

$$T = \frac{1}{3}\left(\overline{u_s'^2}\right) \tag{2.21}$$

where u_s' is the fluctuating solid-phase velocity.

In the above equations, the term η, which is given by $\eta = (1 + e)/2$, brings in the effect of inter-particle collisions through the coefficient of restitution e. The coefficient of restitution e is a measure of the momentum lost due to interparticle collisions. A perfectly elastic collision is indicated by $e = 1$, while a perfectly inelastic collision is indicated by $e = 0$. The parameters ω, g_0, g_1, and g_2 are closure coefficients adopted from Bolio *et al.* (1995). The parameter ω is given by

$$\omega = \frac{1}{1 + \frac{\lambda_p}{H}} \tag{2.22}$$

where H is the width of the channel, and λ_P is the mean free path of the particles which can be defined as the mean distance travelled by the particle before it collides with another particle. It is obtained from the following relation:

$$\lambda_P = \frac{d_p}{6\sqrt{2}\alpha_s} \tag{2.23}$$

The other closure coefficients are given by

$$g_0 = \frac{\alpha_0^{1/3}}{\alpha_0^{1/3} - \alpha_s^{1/3}} \tag{2.24}$$

$$g_1 = \frac{1}{\eta(2-\eta)g_0}\left[1 + \frac{8}{5}\eta\alpha_s g_0(3\eta - 2)\right] \tag{2.25}$$

and

$$g_2 = \frac{8\alpha_s}{5(2-\eta)}\left[1 + \frac{8}{5}\eta\alpha_s g_0(3\eta - 2)\right] + \frac{768\alpha_s^2 g_0 \eta}{25\pi} \quad (2.26)$$

The solid-phase granular temperature transport equation is modelled based on kinetic theory, which was originally proposed for gases. The theory is used to attribute fluid-like properties to the solid-phase present in the flow. The transport equation was adopted from Bolio *et al.* (1995), and is given by

$$0 = -\frac{\partial}{\partial y}(q_{PT}) - \sigma_{xy}\frac{\partial u_s}{\partial y} - \gamma + I_T \quad (2.27)$$

In equation (2.27), q_{PT} is the pseudo-thermal energy flux vector, γ is the dissipation rate of the pseudo-thermal energy due to inelastic interparticle collisions, and I_T is the turbulence modulation term which will be discussed in the next sub-section. The closure expressions for the energy flux vector, and dissipation are given by

$$q_{PT} = -\lambda(\omega g_3 + g_4)\frac{\partial T}{\partial y} \quad (2.28)$$

$$\gamma = \frac{48}{\sqrt{\pi}}\eta(1-\eta)g_0\alpha_s^2\frac{\rho_s}{d}T^{3/2} \quad (2.29)$$

where λ is the thermal conductivity given by

$$\lambda = \frac{25\sqrt{\pi}d\rho_s\sqrt{T}}{128} \quad (2.30)$$

The other closure coefficients, g_3 and g_4 are specified as follows:

$$g_3 = \frac{8}{\eta(41-33\eta)g_0}\left[1 + \frac{12}{5}\eta^2\alpha_s g_0(4\eta - 3)\right] \quad (2.31)$$

$$g_4 = \frac{96\alpha_s}{5(41-33\eta)}\left[1 + \frac{12}{5}\eta^2\alpha_s g_0(4\eta - 3) + \frac{16}{15\pi}\eta\alpha_s g_0(41 - 33\eta)\right] \quad (2.32)$$

2.3 Turbulence modulation

The turbulence modulation terms are included to simulate the effect of each individual phase on the fluctuating velocity field of the other phase. It represents the effect of the solid-phase on the fluid-phase turbulence and vice versa.

Rao *et al.* (2011) defined turbulence modulation as analogous to the case of convective heat transfer between two immiscible fluids where $2k - k_{sf}$ and $k_{sf} - 3T$ are the temperature differences between the two fluids. They assumed that the solid-phase velocity fluctuation is caused by the fluid-phase turbulence. They also assumed that the particles in the solid-phase are fully elastic, so there is no dissipation of energy due to inter-particle collisions, and the fluid is inviscid. Using this analogy they proposed that

$$I_K = -\frac{\rho_f}{\tau_{sf}}\left(2k - k_{sf}\right) + E_w \tag{2.33}$$

$$I_T = \frac{\rho_f}{\tau_{sf}}\left(k_{sf} - 3T\right) \tag{2.34}$$

where k is the turbulence kinetic energy of the fluid-phase, and T is the solid-phase granular temperature which is indicative of the turbulence kinetic energy of the solid-phase.

In equations (2.33) and (2.34), k_{sf} is the cross-correlation product of the solid and the fluid fluctuating velocities, i.e. $k_{sf} = \overline{u_s' u_f'}$. The expression for k_{sf} varies with different authors: the current study uses the expression derived by Sinclair and Mallo (1998), and is given by,

$$k_{sf} = \sqrt{6kT} \tag{2.35}$$

In equations (2.33) and (2.34), τ_{sf} is the time scale over which energy is transferred. Rao *et al.* (2011) used two distinct time-scales. To account for particles that attenuate turbulence, they used $\tau_{sf} = \tau_D = \frac{\alpha_s}{\beta \alpha_f}$, which is generally referred to as the drag time-scale. For particles that enhance turbulence $\tau_{sf} = \tau_c = \frac{d}{24\alpha_s g_0}\sqrt{\frac{\pi}{T}}$ which is referred to as the collision time-scale. Recall that particles enhance turbulence due to the formation of wakes. The additional term E_w is the wake effect model adapted from Lun (2000). Table 2.1 details the relations in the wake effect model.

Table 2.1: Wake term model correlations, Lun (2000)

$E_w = 12\frac{C_w u_s \mu_t k}{d_p^3}$	
$\mu_t = 0.017 Re_s \mu_f, C_w = \frac{10}{3}$	for $150 \leq Re_s \leq 310$
$\mu_t = 1.2 + 0.000057 Re_s^2 \mu_f, C_w = \frac{24}{3}$	for $310 \leq Re_s \leq 610$
$\mu_t = 0.029 Re_s \mu_f, C_w = \frac{24}{3}$	for $Re_s \geq 610$

2.4 Boundary Conditions

The mathematical model introduces transport equations for the fluid-phase and the solid-phase. Wall boundary conditions are defined for each set of transport equations. The boundary conditions defined at the walls for the channel are discussed in the section below.

2.4.1 Fluid-phase boundary conditions:

At the wall the fluid-phase velocity boundary conditions are specified as per the two-layer formulation. For a rough wall, the wall boundary conditions defined for the mean velocity, turbulence kinetic energy and the dissipation rate are:

$$\left(\upsilon_{ef} + \upsilon_t\right)\frac{\partial u_f\big|_{wall}}{\partial y} = u_\tau^2 \tag{2.36}$$

$$k|_{wall} = \frac{u_\tau^2}{\sqrt{C_\mu}} min\left[1; \left(\frac{r_+}{90}\right)^2\right] \tag{2.37}$$

$$\alpha_f \varepsilon\big|_{wall} = \alpha_f \frac{u_\tau^4}{\upsilon_{ef} C_l A_\varepsilon \sqrt{C_\mu}}\left(\frac{r_+}{90 y_o}\right)^2 + I_k \tag{2.38}$$

For a smooth wall, the wall boundary conditions for the mean velocity, turbulence kinetic energy and the dissipation reduce to:

$$u_f\big|_{wall} = 0 \tag{2.39}$$

$$k|_{wall} = 0 \tag{2.40}$$

$$\alpha_f \varepsilon|_{wall} = \alpha_f \upsilon_{ef} \frac{\partial^2 k}{\partial y^2} + I_k \tag{2.41}$$

2.4.2 Solid-phase boundary conditions:

At the wall, the solid-phase particles impinge on the wall and then rebound. The wall boundary conditions for the solid-phase as originally formulated by Sinclair and Jackson (1989) were adopted in the work of Bolio *et al*. (1995). The boundary conditions formulated by Sinclair and Jackson (1989) were based on the work of Hui *et al.* (1984) and Johnson and Jackson (1987). The boundary condition for the solid-phase velocity is obtained by equating the solid-phase shear-stress near the wall to the momentum flux exchanged between the particles and the wall by particle-wall collisions, and is given by

$$\sigma_{xy} = \frac{\rho_s \pi \alpha_s \phi \sqrt{T}}{2\sqrt{3}\left(\frac{\alpha_0}{\alpha_s} - \frac{\alpha_0^{2/3}}{\alpha_s^{2/3}}\right)} \tag{2.42}$$

When the above equation is substituted into equation (2.19), the resulting boundary condition for the solids velocity gradient at the wall is:

$$\left.\frac{\partial u_s}{\partial y}\right|_{wall} = -\frac{48\sqrt{\pi}\phi \alpha_s g_0 u_s|_{wall}}{5\sqrt{3} d_p \alpha_0 (\omega g_1 + g_2)} \tag{2.43}$$

In equations (2.42) and (2.43), ϕ represents the specularity coefficient, which specifies the nature of particle-wall collisions. The value of ϕ varies between ϕ = 0 for perfectly specular collisions and ϕ = 1 for perfectly diffuse collisions. Recall the nature of these collisions can be used to characterize the surface roughness.

The boundary condition above is used to close the set of equations related to the particle momentum transport equations by specifying the solids velocity gradient at the wall.

The boundary condition for granular temperature is obtained by equating the energy flux term q_{PT} to the energy conducted to the wall by the particle-wall collisions and the energy dissipated at the wall due to collisions between the particles and the wall.

It is given by

$$q_{PT} = \frac{\sqrt{3}\rho_s \pi (1-e_w^2) T^{3/2}}{4\left[\left(\frac{\alpha_0}{\alpha_s}\right) - \left(\frac{\alpha_0}{\alpha_s}\right)^{2/3}\right]} - \frac{\rho_s \pi \upsilon^2 \phi \sqrt{T}}{2\sqrt{3}\left[\left(\frac{\alpha_0}{\alpha_s}\right) - \left(\frac{\alpha_0}{\alpha_s}\right)^{2/3}\right]} \tag{2.44}$$

When equation (2.44) is substituted into Equation (2.29), the resulting boundary condition for the granular temperature gradient at the wall is obtained

$$\left.\frac{\partial T}{\partial y}\right|_{wall} = \left(\frac{\phi u_s^2|_{wall}}{\sqrt{3}} - \frac{\sqrt{3}(1-e_w^2)T|_{wall}}{2}\right)\frac{64\sqrt{\pi}\alpha_s g_0}{25\alpha_0 d_p(\omega g_3 + g_4)} \tag{2.45}$$

The boundary condition above is applied to close the set of equations for the granular temperature transport by specifying the granular temperature gradient at the wall.

2.5 Numerical Method

The equations were solved for a 1D horizontal channel using a non-uniform Cartesian grid to obtain time-averaged solutions. In order to obtain a grid independent solution, the mathematical model was tested for various numbers of control volumes. The mean velocity predictions were observed to be identical for grids using 200 and 190 control volumes. This indicates that at 200 control volumes, the solution has become grid independent. Therefore, a grid consisting of 200 control volumes was used for all the calculations reported in the next chapter.

The overall mathematical model consists of five coupled transport equations for the fluid velocity u_f, solid velocity u_s, turbulence kinetic energy *k*, dissipation of turbulence kinetic energy *ε*, and granular temperature *T*, and an algebraic equation used to solve for the solids volume fraction α_s. For solving the set of equations discussed above, there are two major steps that are taken into consideration.

1) Discretization:

To numerically solve the equation set, the partial differential equations were first discretized. Discretization converts the differential equations into linear algebraic equations. The discretization followed the finite volume method of Patankar (1980). The discrete form of the equations were obtained by integrating the differential equations over a generic control volume.

2) Solution:

The discretized transport equations were solved simultaneously using the Tri-Diagonal Matrix Algorithm (TDMA), while a pseudo-transient solution method was used to provide relaxation. Boundary conditions are implemented to solve the discretized transport equations.

To obtain the solids volume fraction, a linearized algebraic equation for α_s is solved. The algebraic equation is based on the transverse momentum equation balance (refer to Equation 2.19). An iterative technique is applied to match the overall mass loading which is related to the bulk solids volume fraction. The mass loading is calculated from the solids volume fraction using the relation:

$$m = \frac{\rho_s \sum \alpha_s u_s \Delta y}{\rho_f \sum (1-\alpha_s) u_f \Delta y} \tag{2.46}$$

As such the mass loading *m* is a function of the particle density, the solids volume fraction, the solids velocity, the fluid density and the fluids velocity.

The initial solution was iterated in time until convergence was obtained for the solution field. The convergence criterion specified was given by

$$\frac{\sigma_{new} - \sigma_{old}}{\sigma_{old}} < 10^{-4} \tag{2.47}$$

where σ stands for the specific variable being solved, the subscript 'new' indicates the present value of σ, and the subscript 'old' indicates the value of σ at the previous iteration level.

CHAPTER 3: COMPUTATIONAL PREDICTIONS FOR PHASIC INTERACTIONS

The following chapter documents the outcomes of the simulations conducted. This study considers fully-developed turbulent gas-solid flow in a horizontal channel. The horizontal orientation introduces an element of asymmetry to the flow due to the force of gravity being transverse to the flow direction. It is to be noted that the channel width considered for all the simulations is H = 35 mm.

Section 3.1 focuses on the behavior of the gas-solid flow in a hydrodynamically rough channel. Previous research done by Yerrumshetty (2007) and Zaman (2013), explored turbulent gas-solid flow in both smooth and rough pipes and are considered a benchmark cases for the current study. The predictions of the turbulent gas-solid flow in a hydrodynamically rough channel are compared to the predictions of a similar flow in a hydrodynamically smooth channel.

Section 3.2 focuses on the behavior of gas-solid flow in a hydrodynamically smooth horizontal channel. However, the channel wall is rough from a particle perspective. To reproduce the effect of roughness on the particles, the particle phase boundary condition introduced by Johnson and Jackson (1987) is used. The flow predictions are compared to the experimental data of Sommerfeld and Kussin (2004).

Section 3.1 and 3.2 present the effect of smooth and rough wall conditions on a gas-solid flow. The turbulent gas-solid flow is affected by the specularity coefficient ϕ, particle mass loading m and the particle Stokes number St. The specularity coefficient describes the nature of the particle-wall interactions. The particle mass loading is defined at the ratio of the solid-phase mass flow rate to the fluid-phase mass flow rate. It is a measure of the solids volume fraction in the channel; a higher mass loading implies a higher number of particles present in the flow. The Stokes number is indicative of the particle's ability to respond to the flow based on the inertia of the particle. Section 3.3 documents a parametric study designed to explore the effect of the specularity coefficient, particle mass loading and particle Stokes number on the particle phase present in the gas-solid channel flow.

3.1 Hydrodynamically rough flow conditions

Geometric roughness in a channel affects both the fluid and the particles present in the flow. The fluid-phase is affected by the change in hydrodynamic drag. The current section explores the effect of roughness by simulating a turbulent gas-solid flow in a hydrodynamically rough channel. The predictions are compared to the predictions of a similar flow in a hydrodynamically smooth channel. For simulating a hydrodynamically smooth wall, the equivalent roughness length and non-dimensionalized roughness height were set to zero. For defining a rough wall, an equivalent roughness length of $y_0^+ = 1.8$ and non-dimensionalized roughness height $r^+ = 90$ were selected based on the model of Durbin *et al.* (2001). In both simulations, for the rough wall as well as the smooth wall, a bulk fluid velocity of $U_{av} = 20$ m/s, a Reynolds number of $Re = 9.3 \times 10^4$, a particle mass loading $m = 0.5$, and a specularity coefficient of $\phi = 0.005$ were used for a particle size of 195 μm.

Figure 3.1 depicts the fluid-phase velocity predictions for the channel with a fully rough wall, compared to the predictions for a hydrodynamically smooth channel. For the rough channel, when compared to the smooth channel, the velocity is lower near the wall and higher in the core region. Roughness enhances the hydrodynamic drag, which slows down the fluid in the near-wall region of the rough channel. To maintain the same bulk velocity a higher pressure gradient is required to overcome the drag created by the roughness of the wall. Hence, a higher fluid velocity is observed at the center of the channel with rough walls due to the higher pressure gradient applied.

Figure 3.2 depicts the non-dimensionalized fluid-phase velocity predictions for the rough and the smooth channel together with the canonical log law for a smooth wall. The fluid-phase velocities are non-dimensionalized using the respective friction velocities and plotted versus the dimensionless wall normal distance $y^+ = \frac{yu_\tau}{\nu}$; only the velocity profile in the lower half of the channel is shown since the velocity field is symmetric. Figure 3.2 shows a shift between the smooth and rough wall profiles, called the roughness shift Δu^+. The roughness shift depends on the non-dimensionalized roughness height and represents the drag created by the wall roughness.

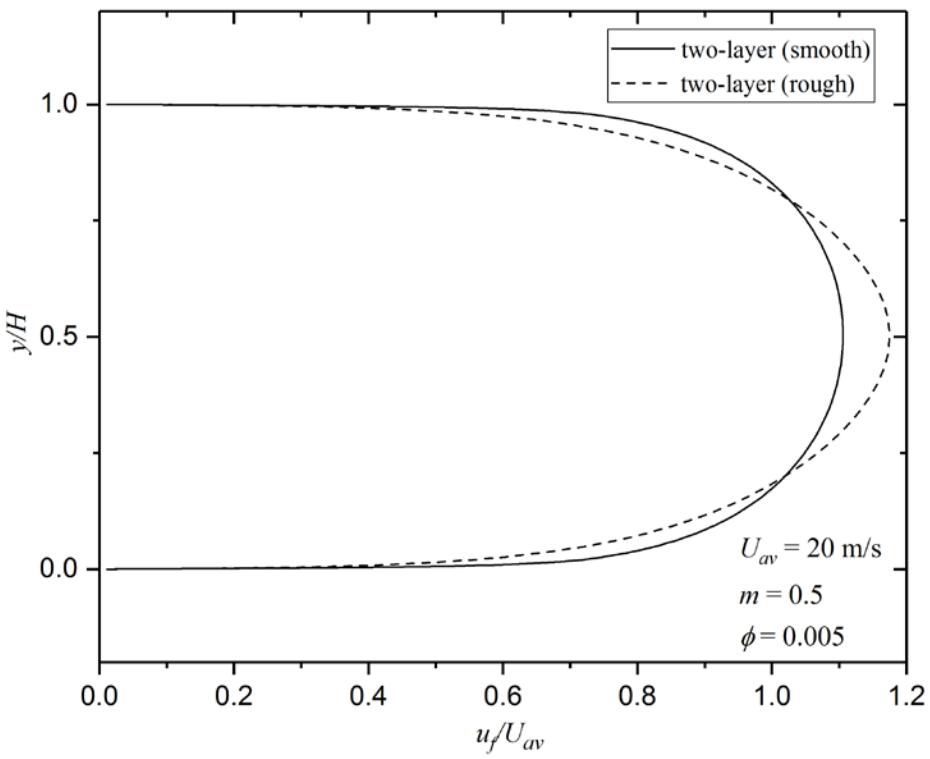

Figure 3.1: Fluid-phase velocity for fully rough flow

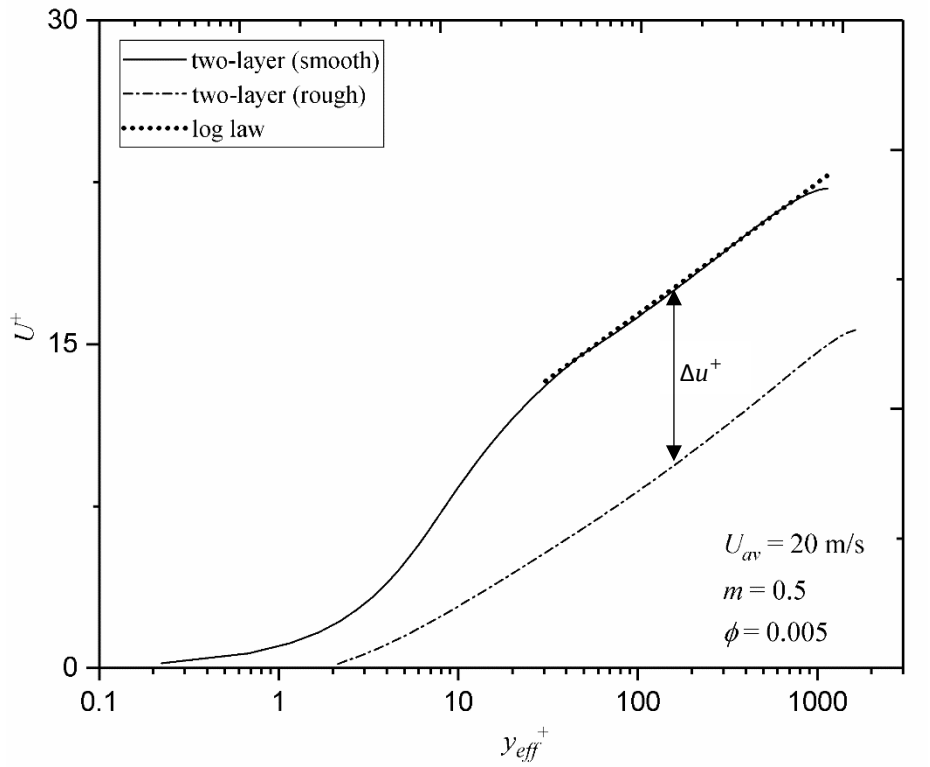

Figure 3.2: Fluid-phase velocity using inner coordinates

Figure 3.3 depicts the eddy viscosity predictions for the flow in the channel with rough walls compared to the eddy viscosity predictions in a smooth channel; a clear-gas eddy viscosity profile for a smooth channel is also added for comparison. The eddy viscosity for the rough channel peaks at $y = 0.25\ H$ and $y = 0.75\ H$. The peak values of the eddy viscosity for the rough channel are approximately 35% higher than the predictions for the smooth wall. A higher eddy viscosity is observed because of a higher shear stress in the near wall region due to the wall roughness. The eddy viscosity profile for the clear-gas follows a similar trend to that of the smooth channel near the wall. However, it peaks at $y = 0.25\ H$ and $y = 0.75\ H$, whereas the eddy viscosity profile for the smooth channel with particles peaks at the center of the channel. The observed peak at center of the smooth channel may be due to the increase in turbulence kinetic energy through the turbulence modulation. Note that the decrease in eddy viscosity at the center of the rough channel is less than the decrease in eddy viscosity at the center of the smooth channel for the clear-gas case.

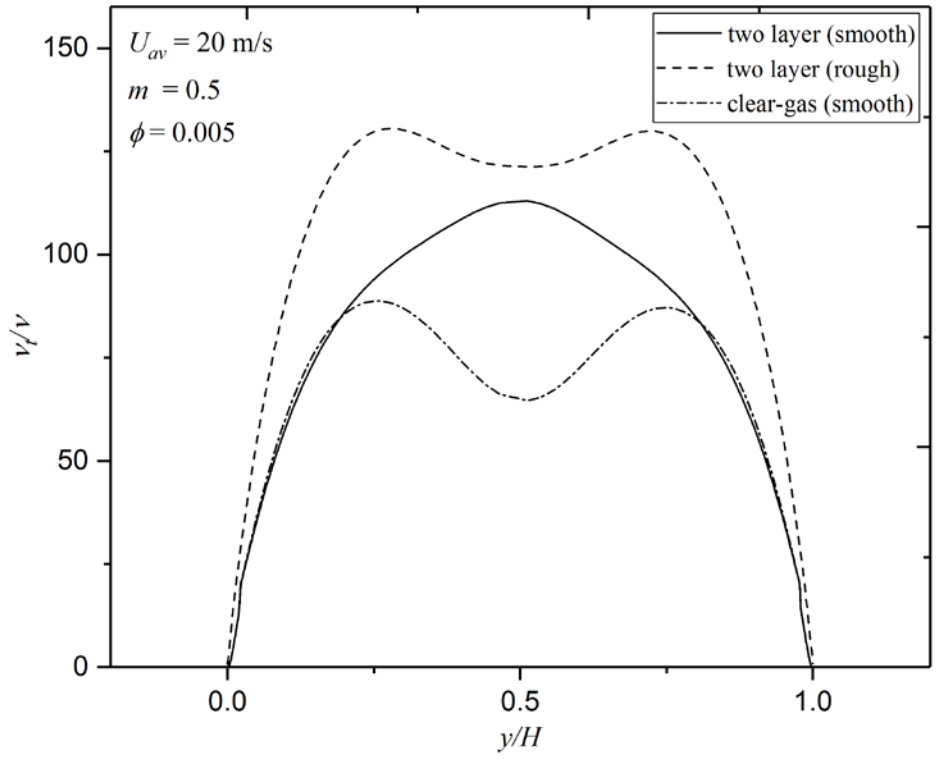

Figure 3.3: Eddy viscosity predictions for fully rough flow

Figure 3.4 depicts predictions for the Reynolds shear stress in the rough channel compared to a smooth channel. Surface roughness marginally increases the fluid shear stress in the near-wall region. The peaks indicating the maximum shear stress occur close to the wall for both the rough and the smooth channel. The difference in the peaks is approximately 6%.

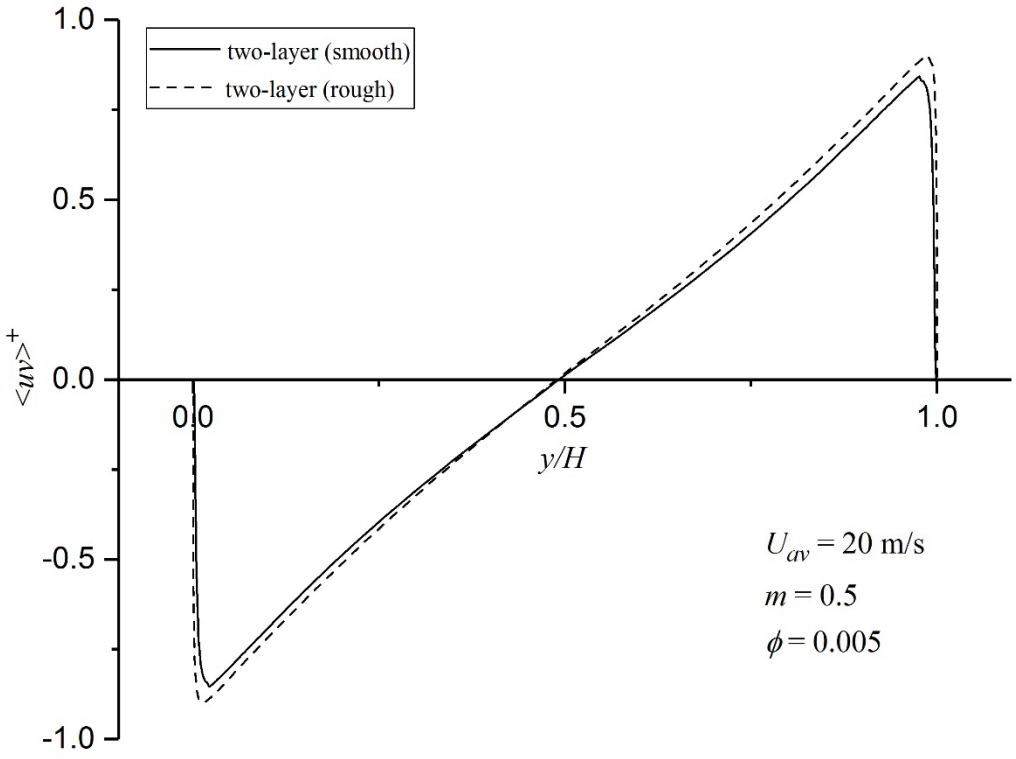

Figure 3.4: Reynolds shear-stress predictions for fully rough flow

Figure 3.5 depicts the predictions for the turbulence kinetic energy in a rough channel compared to the smooth channel case. Note that since the turbulence kinetic energy profiles are symmetric across the channel, only the turbulence kinetic energy profiles for the bottom-half of the channel are presented. The turbulence kinetic energy profile for the rough wall exhibits a peak at the wall; the profile exhibits a second peak at $y^+ = 40$. The turbulence kinetic energy value at the first peak is marginally lower than for the second peak. The non-zero value of the turbulence kinetic energy at the wall is due to the non-zero boundary condition defined by the two-layer model of Durbin *et al.* (2001). The peak value of the turbulence kinetic energy for the smooth channel is higher than for the rough channel; the turbulence kinetic energy is higher in the core region of the rough channel than for the smooth channel. This indicates that roughness tends to homogenize and

enhance the fluid-phase fluctuations across the channel. Note that the turbulence kinetic energy for the rough wall at the center of the channel is lower than for the smooth wall. This may be due to the higher friction velocity used to non-dimensionalize the turbulence kinetic energy for the rough wall.

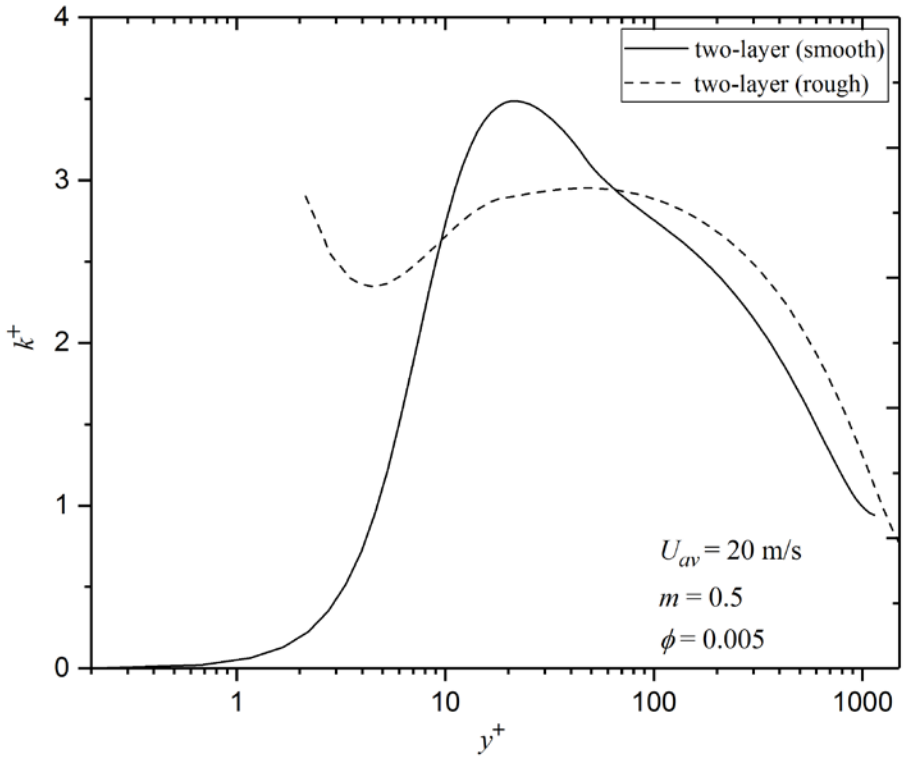

Figure 3.5: Turbulence kinetic energy predictions for fully rough flow

Figure 3.6 depicts the predictions for the solids velocity profile in the rough channel compared to the smooth wall case. The solids velocity for the rough channel is slower in the near-wall region compared to the smooth channel. Note that Figure 3.6 exaggerates the difference due to the scaling selected, and the difference between velocities is overall minimal. The drag due to the roughness reduces the velocity of the particles being conveyed by the fluid. The solids velocity at the center of the rough channel is higher than for the smooth channel. Recall that to maintain the same bulk velocity across the channel a higher-pressure gradient was applied. Hence, a higher fluid velocity is observed at the center of the channel with rough walls, which translates into a higher velocity for the particle-phase being conveyed by the fluid. For both the rough and smooth channel, the solids velocity in the top half of the channel is higher than the solids velocity in the bottom of the

channel. This is because the solids shear stress (refer to Figure 3.9) created by the particles at the upper wall is lower than for the bottom wall.

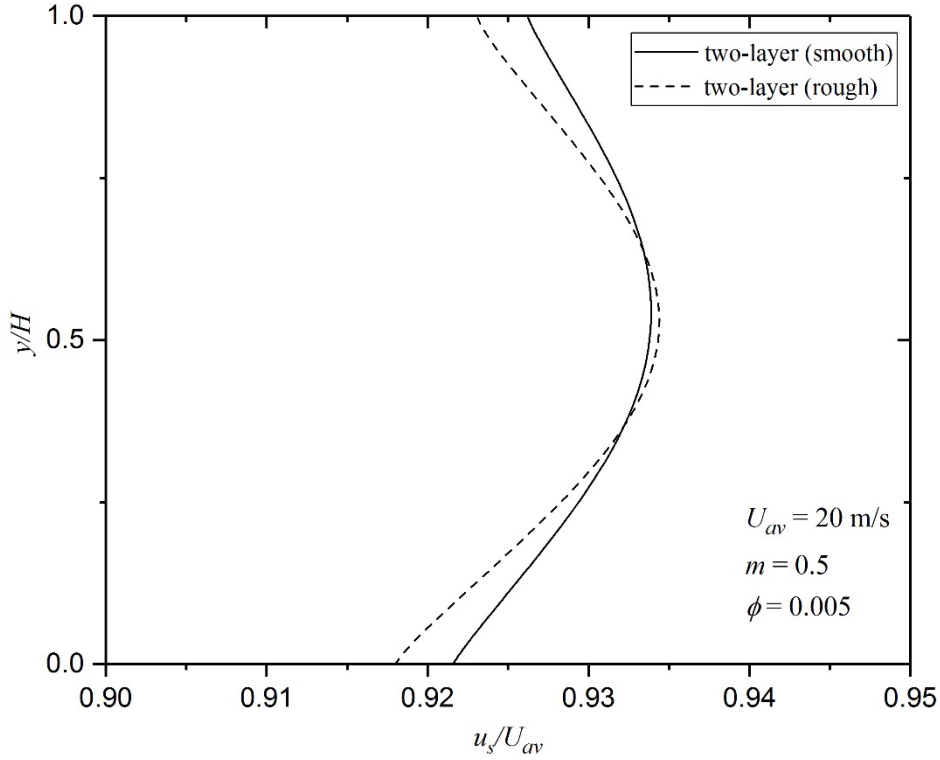

Figure 3.6: Solids velocity predictions for fully rough flow

Figure 3.7 depicts the predictions for the solids volume fraction for the rough channel compared it to the smooth wall case. Also included is the solids volume fraction profile for the flow in a smooth channel without the effect of gravity. In the absence of gravity, the particle distribution across the channel is symmetric, with a majority of the particles distributed in the center of the channel. However, with gravity acting transverse to the flow, a departure from symmetry is observed: the particle distribution now tends to move towards the bottom of the channel. Note that Figure 3.7 exaggerates the difference between the predictions for the solids volume fraction for the rough and the smooth channel. In comparison to the smooth channel, the particle concentration in the rough channel increases by 2% at the top wall and by 1.5% at the bottom wall, while the peak in the bottom-half of the channel reduces by 1.2%. Hence, the distribution of particles becomes slightly more uniform. Due to the increase in granular temperature (see Figure 3.8) the particles for the rough channel are more energized and tend to distribute more evenly across the channel resulting in a slightly higher particle concentration near the walls.

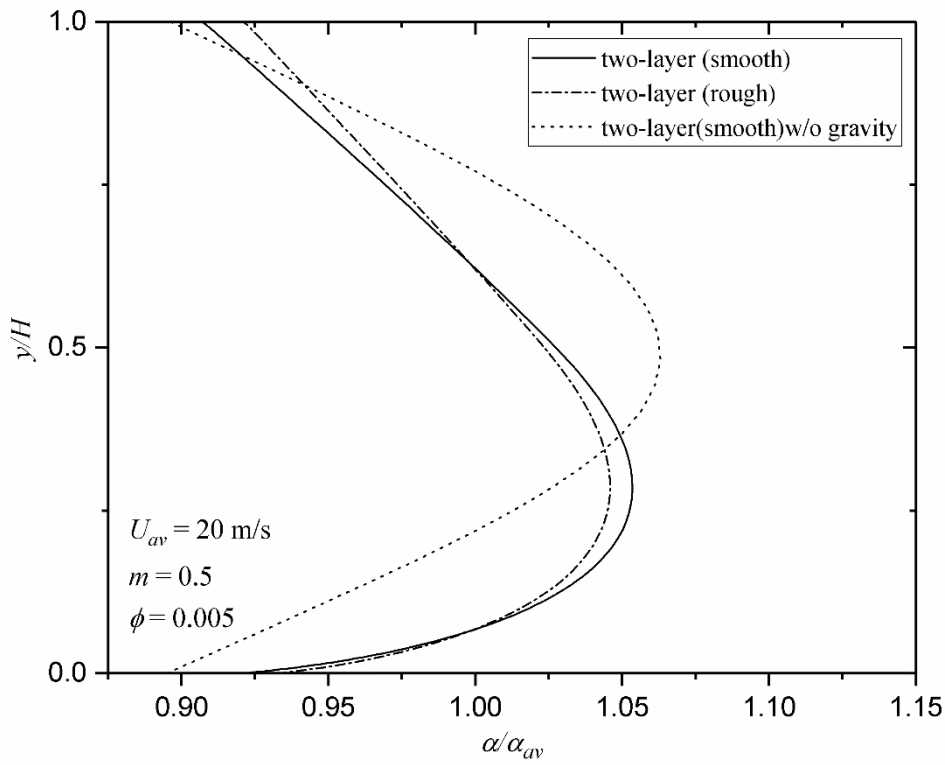

Figure 3.7: Solids volume fraction prediction for fully rough flow

Figure 3.8 depicts the predictions for granular temperature in the rough channel compared to the smooth channel case. The level of the granular temperature in the rough channel is approximately 15% higher than the granular temperature in the smooth channel. Roughness energizes the flow by increasing the turbulence kinetic energy which enhances the granular temperature via the turbulence modulation. The granular temperature for both the rough and smooth channels are observed to attain a maximum at the walls and a minimum at the center of the channel. There are two possible reasons for this observation. The first reason is that the production of granular temperature is maximum at the wall due to the particle-wall collisions. The second reason is that the turbulence kinetic energy peaks at the near-wall region which enhances the granular temperature via the turbulence modulation.

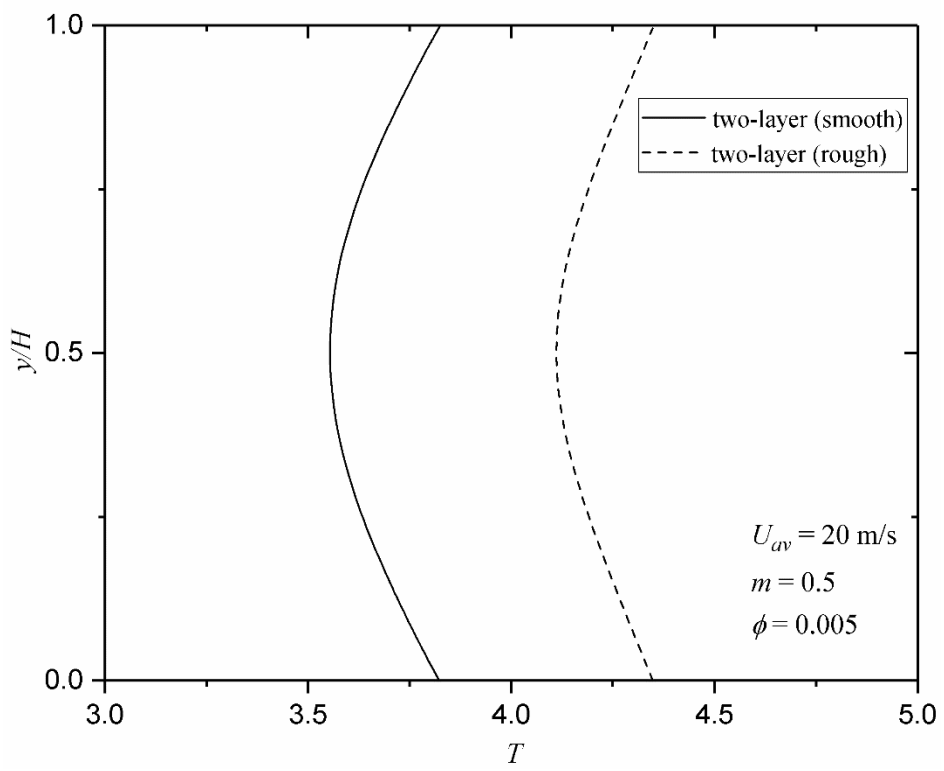

Figure 3.8: Granular temperature prediction for fully rough flow

Figure 3.9 depicts predictions of the solids shear stress for the rough channel compared to the smooth channel. The solids shear stress for both the rough and smooth channel peak close to the wall. Recall that the solids shear stress is coupled to the solids velocity gradients, the reduction in the solids velocity gradient near the wall (see Figure 3.6) results in a reduction in the solids shear stress. In terms of peak values, wall roughness results in a 52% increase in the solids shear stress compared to the smooth channel. The hydrodynamic roughness in the channel creates a higher granular temperature through the turbulence modulation, which results in a higher shear stress. The solids shear stress for both the rough and the smooth channel differ at the wall: the prediction for the top wall is 45% lower than the prediction for the bottom wall. This is due to solids volume fraction being higher at the lower wall than the upper wall. The solids shear stress at the wall for the rough and smooth channels is identical. Recall the specularity coefficient was kept constant at ϕ = 0.005, which implies that the value of the specularity coefficient strongly affects the solids shear stress at the wall.

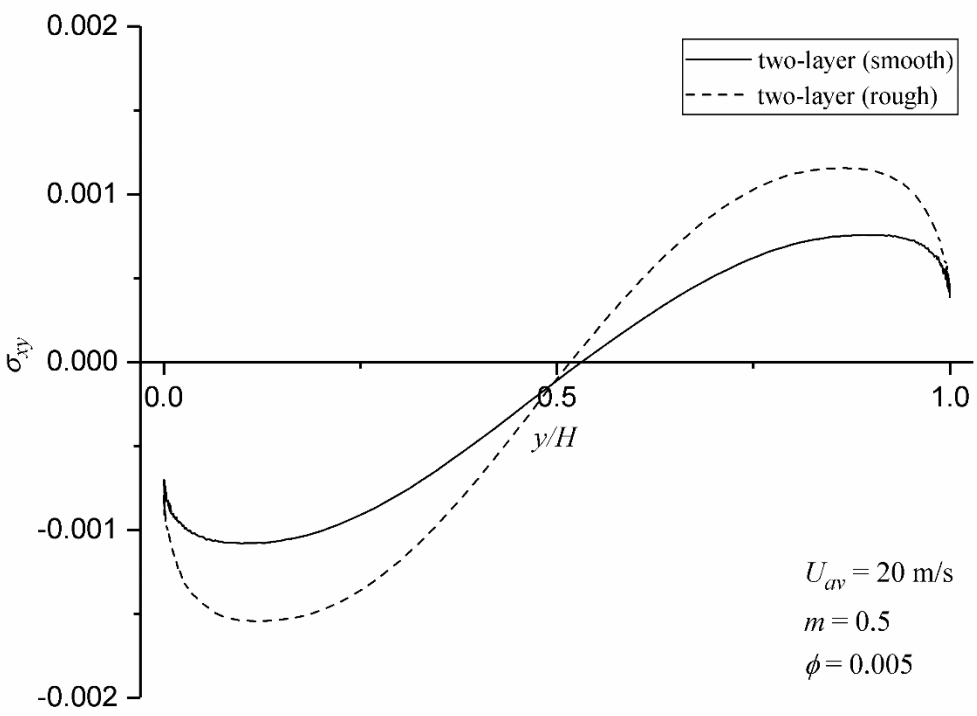

Figure 3.9: Solids shear stress predictions for fully rough flow

The fluid phase and the solid phase in a gas-solid flow interact with each other through two mechanisms. Figure 3.10 depicts a graphic of the interactions between the phases. The fluid-phase velocity interacts with the solid-phase velocity through the particle drag term, while the turbulence kinetic energy interacts with the granular temperature through the turbulence modulation term. The interaction mechanisms are clearly demonstrated in the simulations above irrespective of the surface roughness involved. The channel roughness increases the hydrodynamic drag on the fluid-phase, which reduces the fluid velocity near the wall, and enhances the turbulence kinetic energy and the Reynolds shear stress. The effect of roughness on the fluid-phase velocity is also reflected in the solids velocity through the drag term. As evidenced in the elevated granular temperature predictions for the rough channel, hydrodynamic roughness energizes the particles present in the flow through turbulence modulation. The volume fraction predictions for the rough channel show a more uniform distribution of particles, i.e. roughness tends to homogenize the particle distribution across the channel. The solids shear stress is elevated, which is generally associated with increased particle-wall and particle-particle interactions. However, since the specularity coefficient remains constant for the simulations, the elevated solids shear stress is not due to increased particle-wall collisions, but due to turbulence modulation.

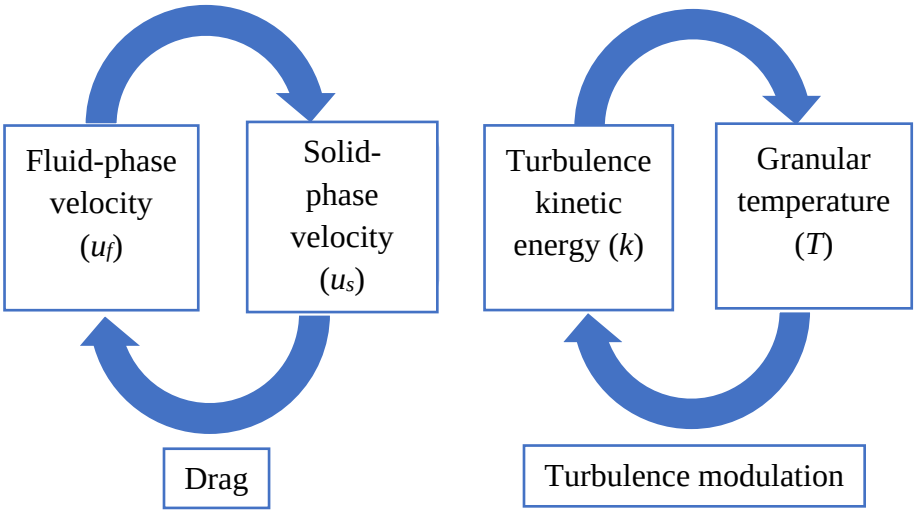

Figure 3.10: Phasic interaction mechanisms

3.2 Effect of wall roughness on particles

This section deals with a rough wall that is hydrodynamically smooth but has a significant effect on the particle collision at the wall. The experimental results of Sommerfeld and Kussin (2004) are used to validate the predictions of the numerical model. Table 3.1 indicates the experimental conditions used for validating the predictions of the numerical model in the study. R_x and R_y indicate the dimensions of the roughness in the stream-wise and wall-normal directions respectively. Sommerfeld and Kussin (2004) used three levels of roughness: R0, R1 and R2, where the height of the roughness R_y increased with each level of roughness. The data selected for the different roughness levels from a more extensive set of experimental results have the same mass loading. From an experimental perspective, mass loading relates to the number of particles fed into the flow per unit time compared to the net volume flow rate of the fluid, both of which are relatively easy to measure and control.

Table 3.1: Experimental conditions (Sommerfeld and Kussin, 2004)

Roughness level	R_x (µm)	R_y (µm)	U_{av} (m/s)	m	Specularity Coefficient (ϕ)
R0	2.32	2.09	20	0.3	0.008
R1	4.26	3.47	20	0.3	0.0101
R2	6.83	6.89	20	0.3	0.0187

Since the roughness levels used here have negligible hydraulic contribution, the two-layer model parameters (y_0, r_+) were set to zero. The roughness, however, affects the particles present in the flow. To simulate the nature of collisions of the particles with the rough channel wall, the specularity coefficient ϕ was set to obtain the best agreement with the solids velocity profiles from the experimental study of Sommerfeld and Kussin (2004). Figure 3.11 depicts a schematic in which the bulk velocity is maintained the same. This ensures the under-predicted area is same as that of the over-predicted area, hence maintaining the same bulk flow rate.

The specularity coefficient in this study was calibrated to ϕ = 0.008, 0.0101 and 0.0187 for roughness levels R0, R1 and R2 respectively. As a point of reference, a specularity coefficient of $\phi = 0.002$ was used by Bolio *et al.* (1995) to simulate gas-solid flow in a pipe with a smooth wall. The particle-wall coefficient of restitution was set to $e_w = 0.9$, while the particle-particle coefficient of restitution was set to $e_p = 0.9$, as per Kussin and Sommerfeld (2002). The bulk fluid-phase velocity was maintained at 20 m/s as per the experimental conditions and the particle size was 195 µm for the spherical glass beads ($\rho_s = 2500\ \mathrm{kg/m^3}$) used in the experiments of Sommerfeld and Kussin (2004).

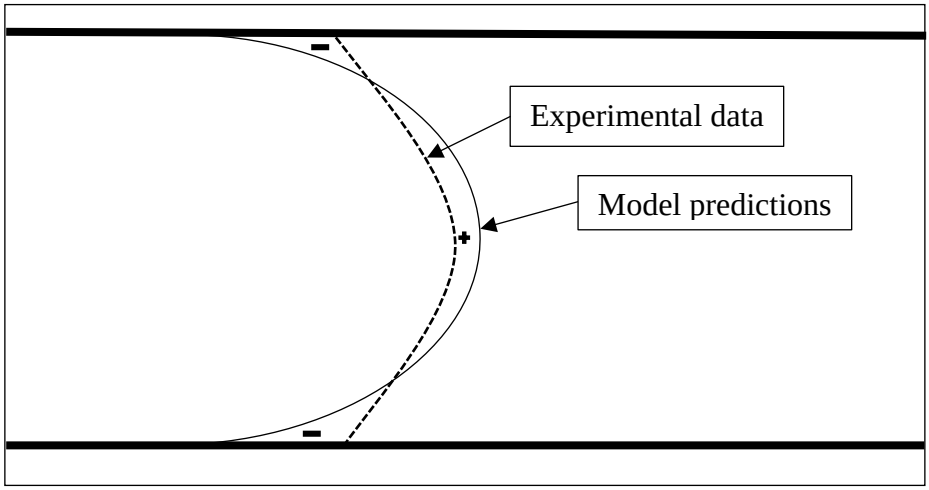

Figure 3.11: Schematic comparison of bulk velocity profiles

Figure 3.12 depicts the predictions for the solids velocity of a gas-solid flow in a channel for the three levels of wall roughness. As discussed previously, the solids velocity predictions were calibrated to the experimental data by tuning the specularity coefficient. The solids velocity predictions for the roughness R0 under-predicts the experimental data at the center of the channel by 0.8% and over-predicts the experimental data in the near-wall region by 5.3%. The solids velocity predictions for the roughness R1 over-predicts the experimental data at the upper wall region of the channel by 1.9% and under-predicts the experimental data in the lower half of the channel by 0.8%. The solids velocity predictions for the roughness R2 closely follows the experimental data of Sommerfeld and Kussin (2004). It is observed that the degree of agreement with the experimental data increases with the level of roughness. The maximum deviation from the experimental data was observed for the solids velocity prediction for roughness R0 in the near-wall region. Note that Kussin and Sommerfeld (2002) report an experimental uncertainty of 3%.

The predicted solids velocity and the experimental data both reduce with increasing levels of roughness, which is due to the increase in solids viscosity (refer to Figure 3.18) with increasing roughness, which in turn increases the wall shear stress of the particle-phase. The experimental profiles become more uniform with increasing levels of roughness. However, the same is not observed in the predicted profiles for the solids velocity. The predicted solids velocity profile, irrespective of the level of roughness, is higher at the upper wall than at the lower wall. This is due to the solids shear stress (refer to Figure 3.19 and Table 3.2) being higher at the lower wall than at the upper wall.

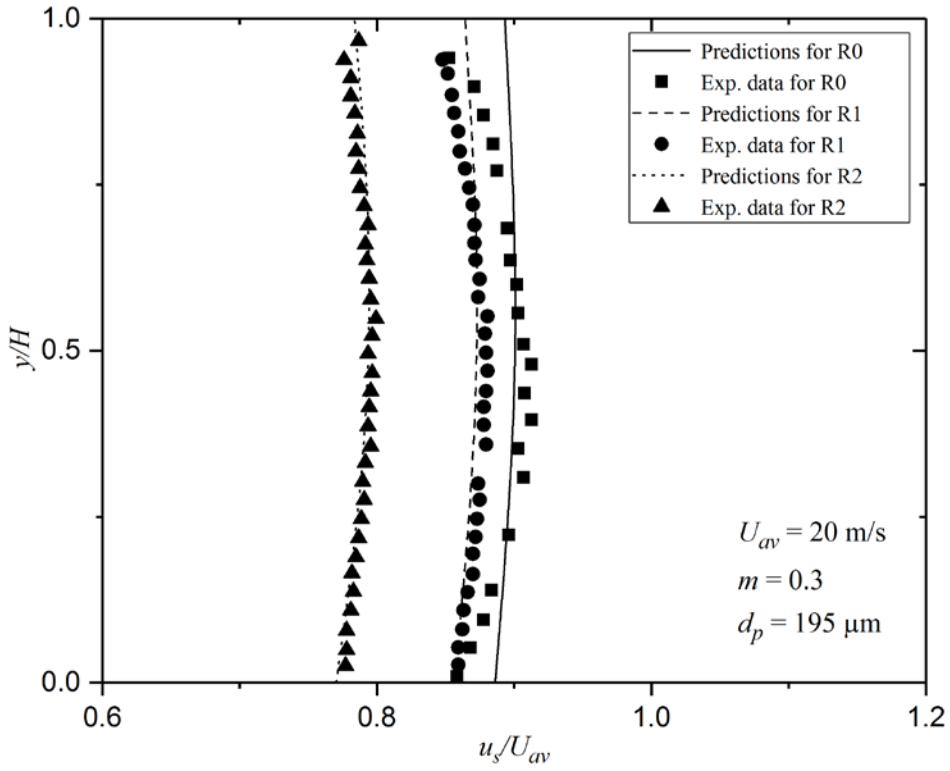

Figure 3.12: Solids velocity predictions for different levels of roughness compared to the experimental data of Sommerfeld and Kussin (2004)

Figure 3.13 depicts the predictions for the normalized solids volume fraction along with the corresponding experimental profiles from Sommerfeld and Kussin (2004). The experimental solids volume fraction profile for the roughness R0 (see Figure 3.13(a)) indicates that the solids volume fraction at the top wall is lower than for the bottom wall. The solids volume fraction gradually increases from the top wall to the near-wall region of the bottom wall. The solids volume fraction profile peaks in the near-wall region; the profile after the peak exhibits a downward trend near the bottom wall. The experimental solids volume fraction profile for the roughness R1 (see Figure 3.13(b)) shows a similar trend to that for the roughness R0. The solids volume fraction profile becomes more uniform; the peak in the profile shifts towards the bottom wall. The experimental solids volume fraction profile for the roughness R2 (see Figure 3.13(c)) shows a more uniform particle distribution; the peak of the profile is located at the bottom wall of the channel. From the experimental profiles, it can be concluded that roughness homogenizes the particle distribution across the channel; the peak in the solids volume fraction profile migrated towards the wall with the increase in roughness.

The predictions for the solids volume fraction for roughness R0 in Figure 3.13(a) is much more homogenous; in comparison to the experimental profiles the predicted solids volume fraction over-predicts at the top wall and under-predicts the peak near the bottom wall. The predictions for the solids volume fraction for roughness R1 in Figure 3.13(b) is nearly identical to that for the roughness R0. In comparison to the experimental profiles the predicted solids volume fraction over-predicts at the top wall and under-predicts the peak near the bottom wall. The predictions for the solids volume fraction for roughness R2 in Figure 3.13(c) is marginally more uniform than for the roughness R0 and R1. This is due to the increase in granular temperature (see Figure 3.17), which energizes the particles present in the gas-solid flow. The solids volume fraction for roughness R2 generally agrees with the experimental profile in Figure 3.13(c) but under-predicts the peak at the bottom of the channel.

Figure 3.14 depicts the predicted profiles for the solids volume fraction for the three different levels of roughness. The magnitude of the bulk solids volume fraction increases with increasing levels of roughness as seen in Table 3.2. The mass loading of a gas-solid flow is expressed as $m = \frac{\rho_s \sum \alpha_s u_s \Delta y}{\rho_f \sum (1-\alpha_s) u_f \Delta y}$. Since the mass flow rate reduces with increasing levels of roughness, to maintain the same mass loading, the bulk solids volume fraction must increase. The solids volume fraction profiles become more uniform with increasing levels of roughness. This is due to the increase in granular temperature (refer to Figure 3.17), which energizes the particles and spreads them more uniformly across the channel.

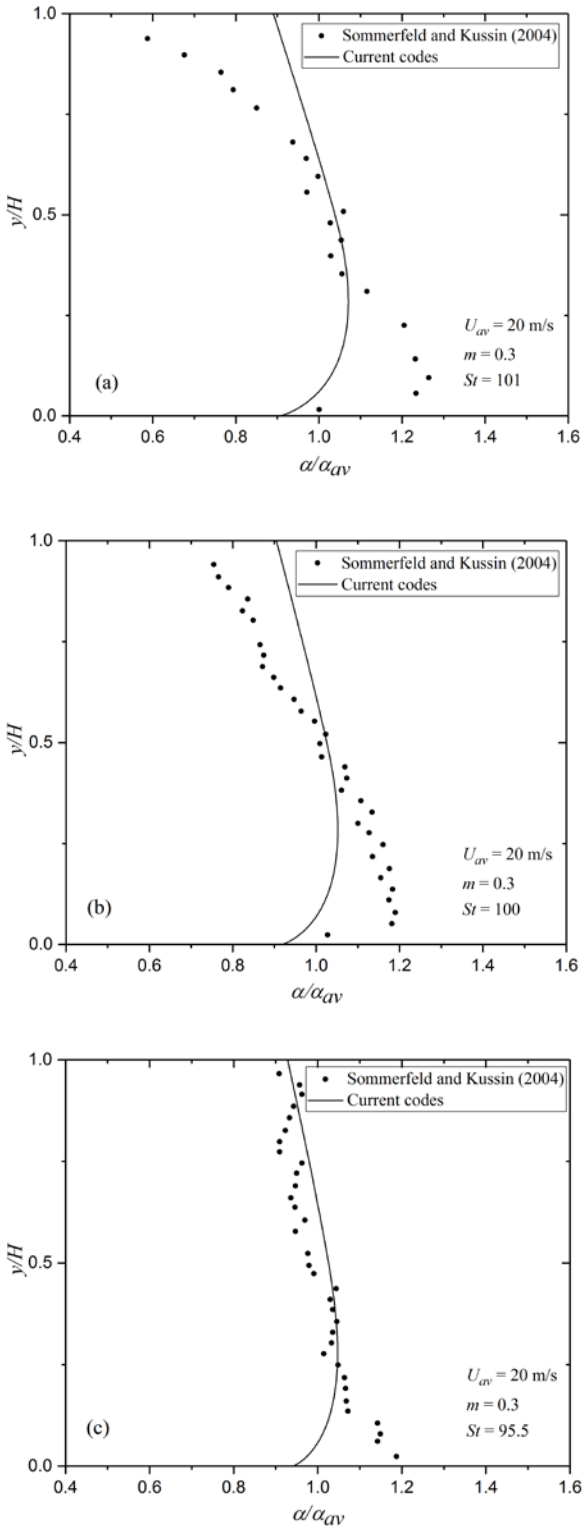

Figure 3.13: Normalised solids volume fraction predictions for different levels of roughness: a) low roughness – R0, b) intermediate roughness – R1, c) high roughness – R2

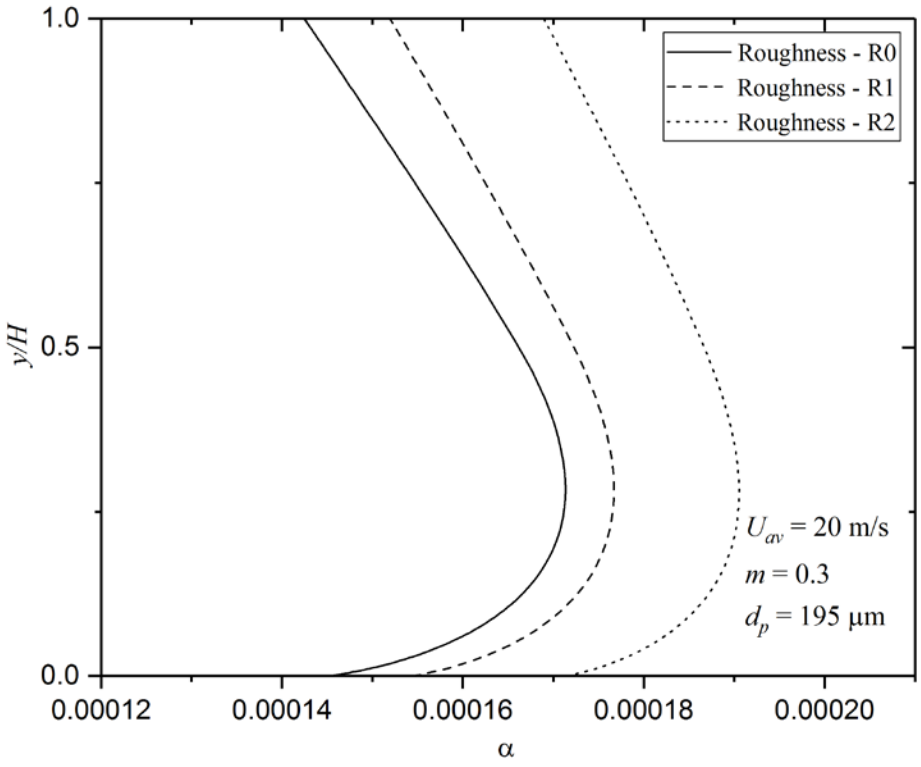

Figure 3.14: Solids volume fraction predictions for different levels of roughness

Table 3.2: Bulk solids volume fraction for different levels of roughness

Roughness level	$\boldsymbol{\alpha_{av}}$
R0	0.0160%
R1	0.0168%
R2	0.0182%

Figure 3.15 depicts the predictions for the turbulence kinetic energy. Note that the turbulence kinetic energy profiles are symmetrical across the channel so only the profile for the bottom half of the channel is presented for each level of roughness. The near-wall peak for the turbulence kinetic energy is almost identical for all three levels of wall roughness. However, at the core of the channel, the predictions for the turbulence kinetic energy are observed to increase with an increase in roughness. This is due to the increase in granular temperature (refer to Figure 3.17)

with increasing roughness; the granular temperature affects the turbulence kinetic energy through the turbulence modulation term.

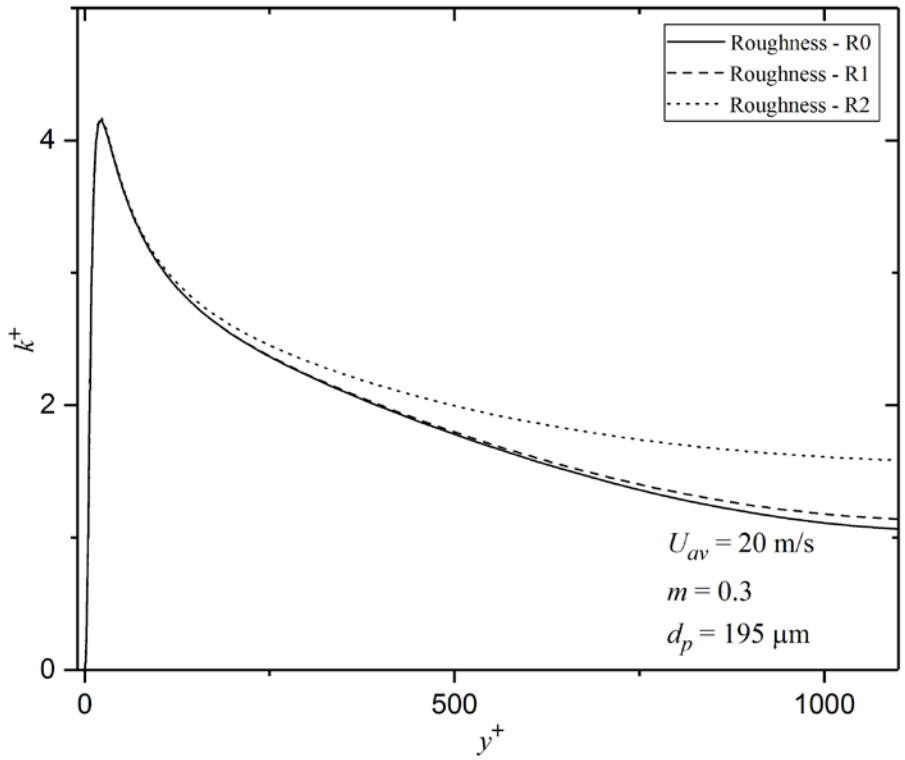

Figure 3.15: Turbulence kinetic energy predictions for different levels of wall roughness

Figure 3.16 depicts the predictions for the granular temperature. The granular temperature for the channel with wall roughness R1 is approximately 11% higher than for roughness R0; the granular temperature with wall roughness R2 is approximately 60% higher than for roughness R1. The increase in granular temperature with increasing roughness implies that roughness energizes the particles in the flow. In each case, the granular temperature is higher at the wall than at the center of the channel. There are two possible reasons for this observation. The first reason is that the net production of granular temperature is maximum at the wall due to the particle-wall collisions. The second reason is that the turbulence kinetic energy peaks at the near-wall region, which enhances the granular temperature via the turbulence modulation.

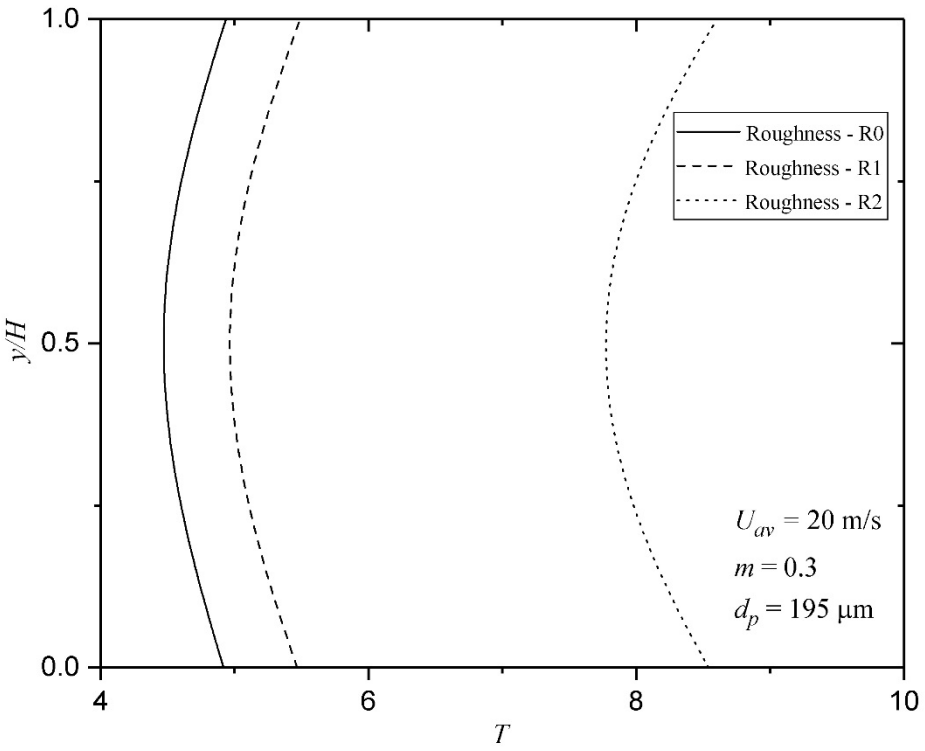

Figure 3.16: Granular temperature predictions for different levels of wall roughness

Figure 3.17 depicts the predictions for the solids viscosity. The solids viscosity at the center of the channel with roughness R1 is approximately 11% higher than for the roughness R0; the solids viscosity at the center with roughness R2 is 38% higher than for the roughness R0. Mathematically, the solids viscosity is a function of the granular temperature, $\mu_s = \frac{5\sqrt{\pi} d_p \rho_s \sqrt{T}}{96}$, which implies that an increase in granular temperature increases the corresponding solids viscosity. The solids viscosity profiles are observed to have a local peak at the top wall while the local peak is located at a finite distance from the wall for the bottom wall.

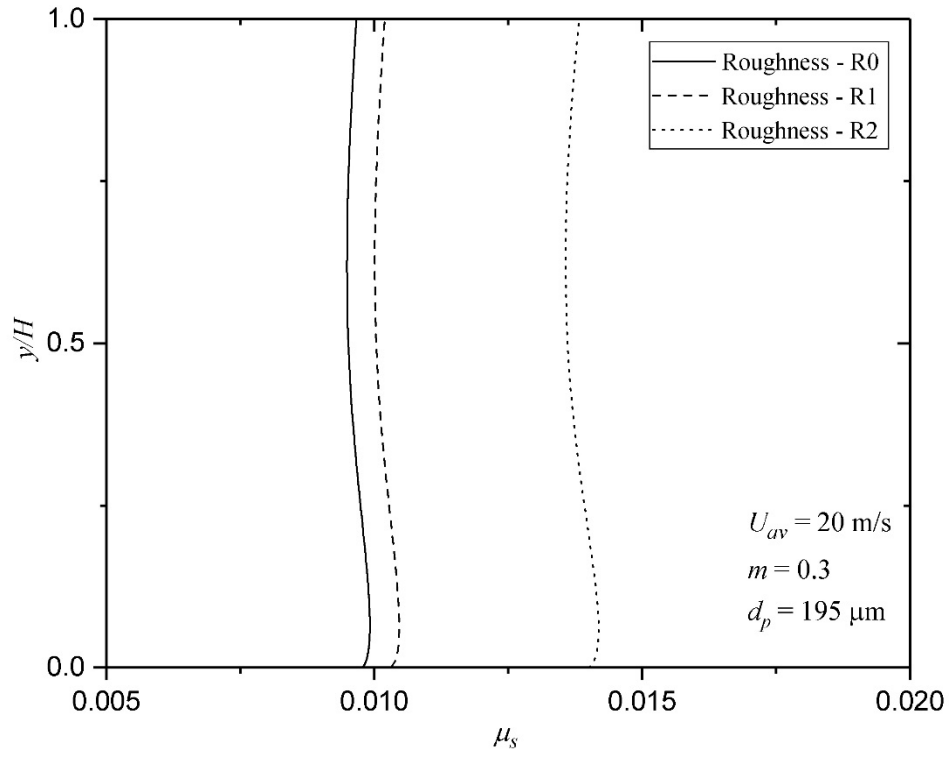

Figure 3.17: Solids viscosity predictions for different levels of roughness

Figure 3.18 depicts the predictions for the solids shear stress. The solids shear stress is observed to increase with increasing roughness. Mathematically, the solids shear stress is a function of the solids viscosity and the solids velocity gradient, $\sigma_{xy} = -\mu_s(\omega g_1 + g_2)\frac{\partial u_s}{\partial y}$, which implies that an increase in granular temperature increases the corresponding solids shear stress. The predicted solids shear stress profiles are asymmetric; the value is higher at the bottom wall of the channel than the upper wall of the channel. The shear stress is closely coupled to the solids volume fraction, and the solids volume fraction is higher at the lower wall than at the upper wall. This translates into a higher shear stress for the bottom wall and a lower shear stress for the upper wall. Table 3.3 lists the wall-shear stress predictions at both channel walls for the three levels of wall roughness. The magnitude of asymmetry (refer to Table 3.3) is observed to increase with an increase in the roughness. This is due to the increased excitation of the particles with increasing roughness levels, as indicated by the elevated granular temperature.

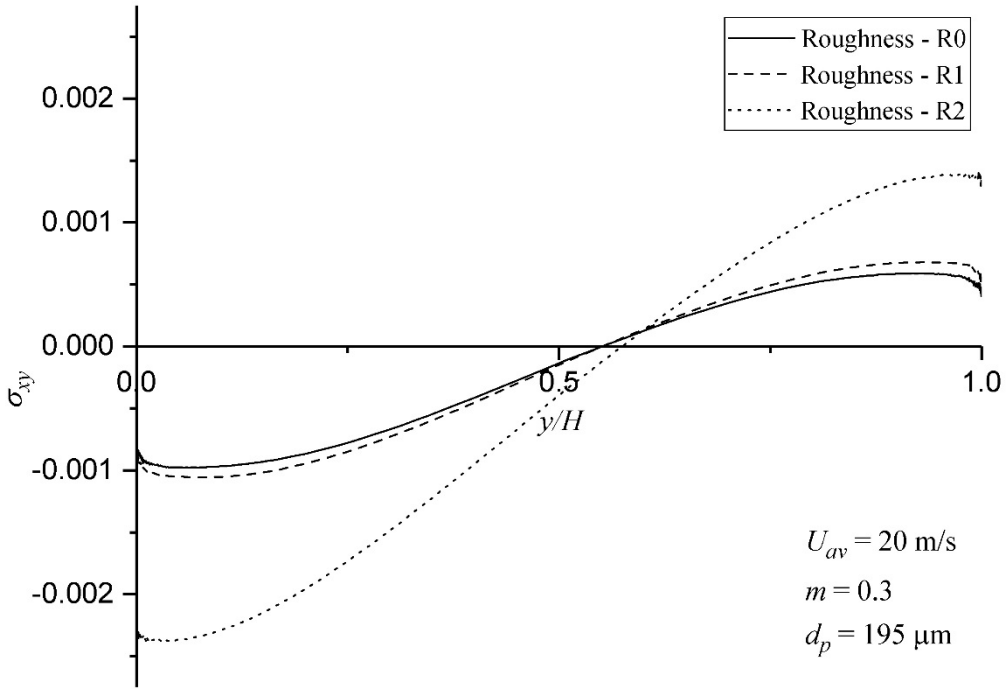

Figure 3.18: Solids shear stress predictions for different levels of roughness

Table 3.3: Solids wall shear-stress predictions for different levels of roughness

Roughness level	$\sigma_{xy,lower\ wall}$	$\sigma_{xy,upper\ wall}$	**difference**
R0	7.68 x 10^{-4}	4.29 x 10^{-4}	3.39 x 10^{-4} (44%)
R1	9.82 x 10^{-4}	5.17 x 10^{-4}	4.65 x 10^{-4} (47%)
R2	2.23 x 10^{-3}	1.32 x 10^{-3}	9.1 x 10^{-4} (41%)

The current study indicates that the specularity coefficient can be tuned to reflect the effects of roughness on the particles. The agreement of the simulations with the experimental data improve with the increase in wall roughness level, which means that specularity coefficient is less effective for a wall with smaller roughness. An increase in roughness makes the particle distribution across the channel more uniform due to the elevated granular temperature. The increase in granular temperature energizes the particles. The energized particles also elevate the solids viscosity predictions, as well as the solids shear stress predictions with increasing levels of roughness. An

enhanced solids viscosity results in a greater resistance to particle flow, which is consistent with the lower solids velocity predicted for increased roughness.

3.3 Sensitivity analysis

Parametric studies were conducted to explore the influence of specific parameters on the particle transport. The particle-phase characteristics in a gas-solid flow depend on the specularity coefficient, mass loading (solids volume fraction), the Stokes number (particle size) and the bulk velocity. For creating a parametric study, the bulk velocity was kept constant for a hydrodynamically smooth horizontal channel, while the specularity coefficient, mass loading, and Stokes number were systematically varied. Table 3.3 shows a matrix giving the range of the values of the parameters used for the simulations. The central column in the matrix indicates the fixed values of parameters during the parametric simulations. For studying the effect of the specularity coefficient, the mass loading was set to m = 0.7, while the Stokes number was set to St = 24. For studying the effect of mass loading, the specularity coefficient was set to ϕ = 0.005, while the Stokes number was set to St = 24. Similarly, for studying the effect of Stokes number, the mass loading was set to m = 0.7, while the specularity coefficient was set to ϕ = 0.005. Note that the mass loading value of m = 0.7 was not used in the parametric study of m.

Table 3.4: Simulation Matrix

$\boldsymbol{\phi}$		0.01	0.005	0.015	0.02
$\boldsymbol{m}$	0.4	0.6	0.7	0.8	1.0
$\boldsymbol{St}$	95	595	24	2315	

Central matrix

3.3.1 Specularity coefficient

The specularity coefficient was initially defined by Johnson and Jackson (1976). Recall, that the specularity coefficient defines the nature of particle-wall interactions by specifying the ratio of the specular to diffuse particle-wall collisions.

To study the effect of the specularity coefficient on the solid-phase flow characteristics, a set of values ranging from ϕ = 0.005 to ϕ = 0.02 were selected. The study attempts to understand the

effect of increasing the number of diffuse particle-wall collisions by increasing the specularity coefficient. The lower value of $\phi = 0.005$ was set to match with the ϕ value used by Yerrumshetty (2007) for simulating gas-solid flows in a smooth vertical pipe. The higher value of $\phi = 0.02$ was selected to closely match with the ϕ value set for the high roughness case in section 3.2. An intermediate mass loading of $m = 0.7$ with a bulk fluid-phase velocity of $U_{av} = 18$ m/s were selected for a particle with Stokes number of $St = 24$.

Figure 3.19 depicts the predictions for the solids velocity profile; it shows a decrease in the solids velocity with an increase in specularity coefficient. The solids viscosity increases (refer to Figure 3.22) with the value of the specularity coefficient which in turn decreases the solids velocity. The solids velocity profile is observed to be slightly asymmetric across the channel: the value at the upper wall is higher than the value at the bottom wall. This is due to the asymmetric profiles for the solids shear stress across the channel (refer to Figure 3.23). The higher shear stress at the bottom wall results in a lower solids velocity, while the lower shear stress at the upper wall results in a higher solids velocity. At $\phi = 0.005$, the solids velocity at the top wall is 2% higher than for the bottom wall; at $\phi = 0.02$, the solids velocity at the top wall is 4% higher than for the bottom wall. This implies that the asymmetry for the solids velocity marginally increases with the value of specularity coefficient. The solids shear stress asymmetry also increases with the value of specularity coefficient which in turn enhances the asymmetry in the solids velocity profiles.

Figure 3.20 depicts the predictions for the solids volume fraction profile. The particle distribution becomes more uniform with an increase in the specularity coefficient. The particle concentrations at the walls also increase. The increase in the specularity coefficient results in a higher granular temperature (refer to Figure 3.21). The particles are more energized with a more homogeneous distribution across the channel as a result of the increase in granular temperature.

Figure 3.21 depicts the predictions for the granular temperature. The granular temperature is observed to increase with an increase in the specularity coefficient. This implies that the increase in the value of the specularity coefficient energizes the particles in the flow. In each case, the granular temperature is higher at the wall than at the center of the channel. There are two possible reasons for this observation. The first reason is that the net production of granular temperature is maximum at the wall due to the particle-wall collisions. The second reason is that the turbulence

kinetic energy peaks in the near-wall region, which enhances the granular temperature via the turbulence modulation.

Figure 3.22 depicts the predictions for the solids viscosity profiles. The solids viscosity increases with an increase in specularity coefficient. Mathematically, the solids viscosity is a function of the granular temperature, $\mu_s = \frac{5\sqrt{\pi}d_p\rho_s\sqrt{T}}{96}$, which implies that an increase in granular temperature increases the corresponding solids viscosity. The solids viscosity profiles are observed to peak at the top wall while a near-wall peak is observed at the bottom wall.

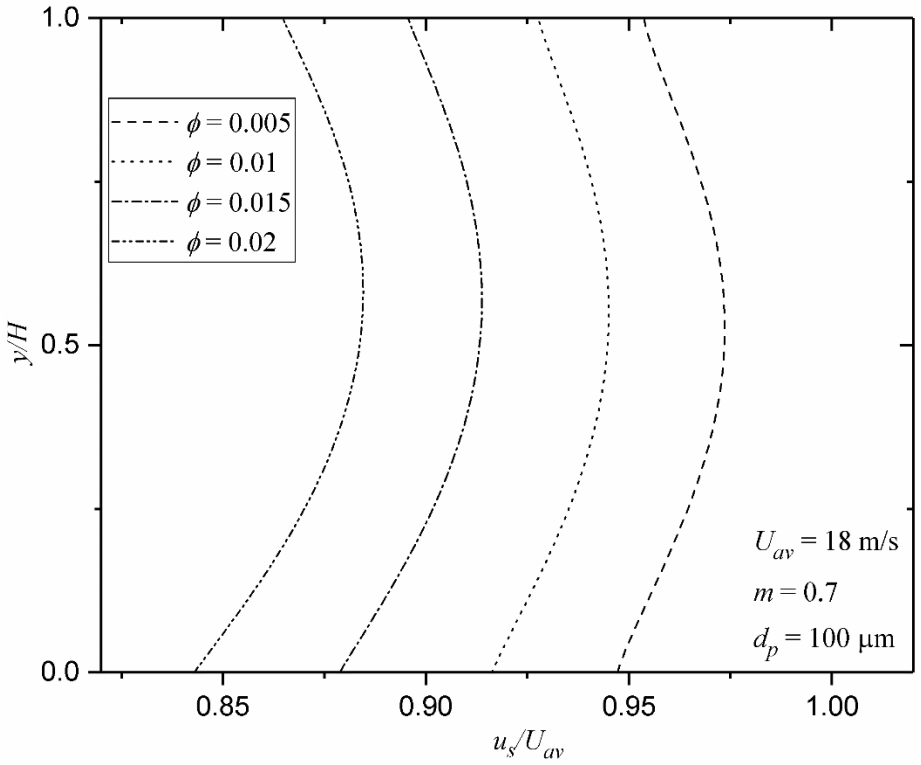

Figure 3.19: Solids velocity predictions for different specularity coefficients

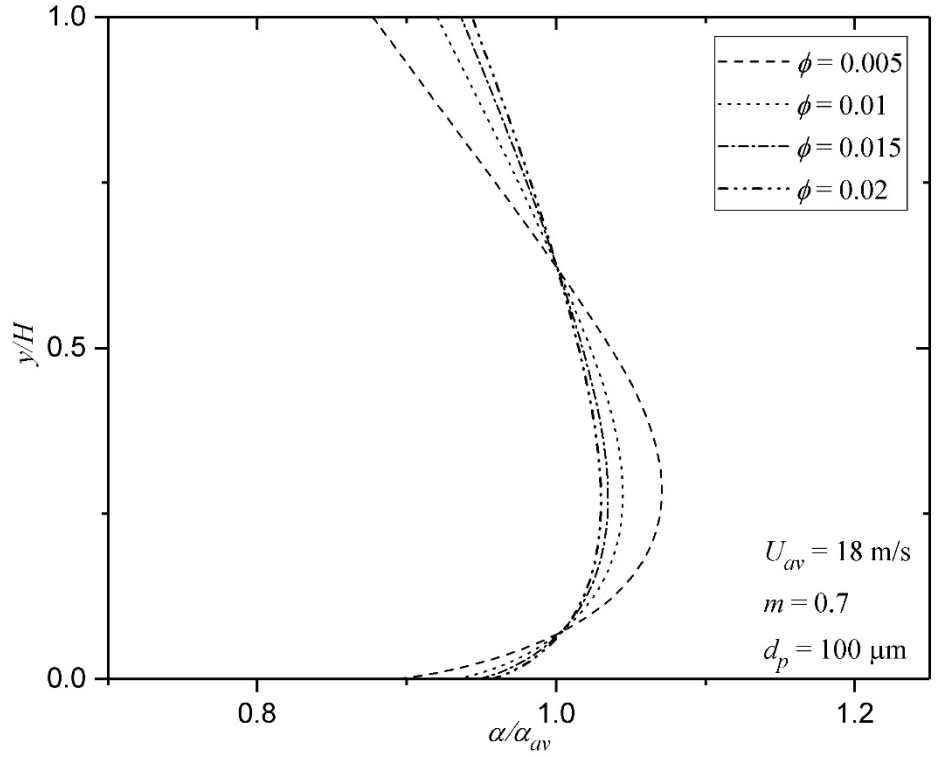

Figure 3.20: Solids volume fraction predictions for different specularity coefficients

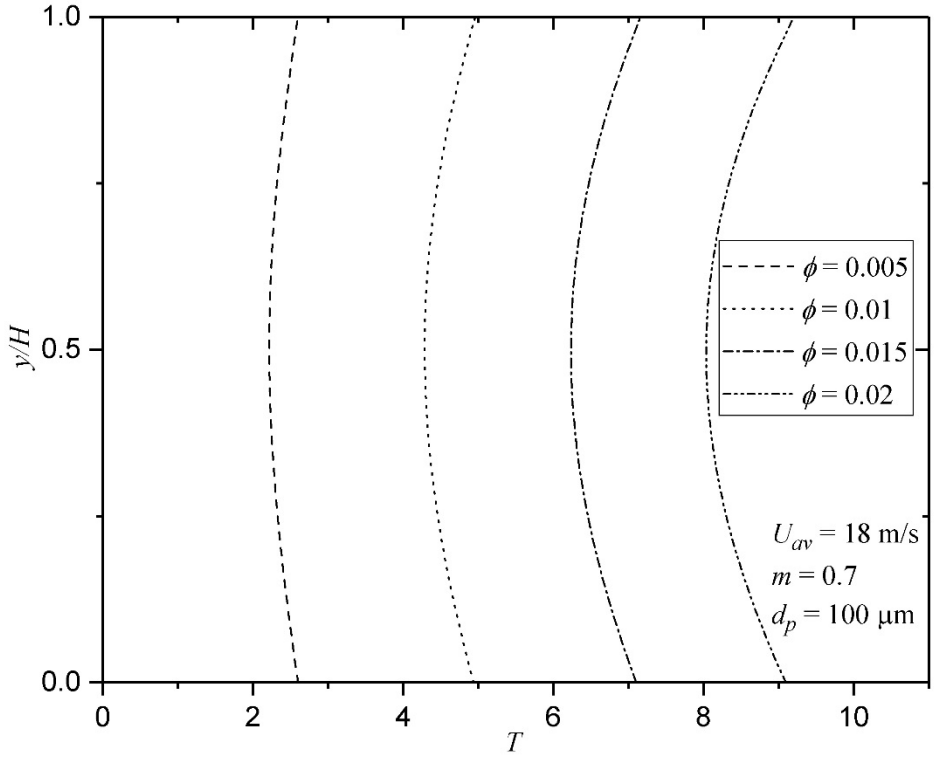

Figure 3.21: Granular temperature predictions for different specularity coefficients

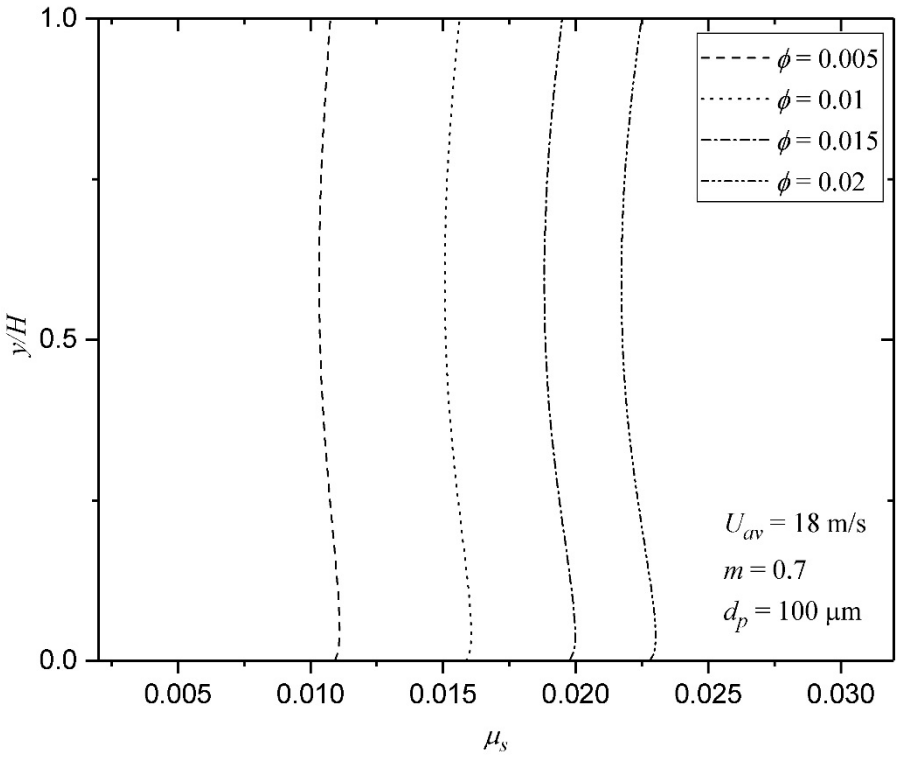

Figure 3.22: Solids viscosity predictions for different specularity coefficients

Figure 3.23 depicts the predictions for the solids shear stress. Table 3.5 shows the value of the peak shear stresses near the top and bottom wall of the channel, as well as the wall shear stress values for the top and bottom-wall of the channel. The solids shear stress increases with an increase in the specularity coefficient. Mathematically, the solids shear stress is a function of the solids viscosity and the solids velocity gradient, $\sigma_{xy} = -\mu_s(\omega g_1 + g_2)\frac{\partial u_s}{\partial y}$, which implies that an increase in granular temperature increases the corresponding solids shear stress. An increase in the specularity coefficient increases the granular temperature which in turn increases the solids shear stress. The shear stress profile is asymmetric as seen in Figure 3.24, which is because the shear stress is closely coupled to the solids volume fraction (refer to Equation (2.18)). The solids volume fraction is higher at the bottom wall of the channel than at the upper wall of the channel, which translates into a higher shear stress near the bottom wall of the channel and a lower shear stress near the upper wall of the channel. The asymmetry of the solids shear stress distribution across the channel increases with increasing specularity coefficient, which is due to the elevated granular temperature.

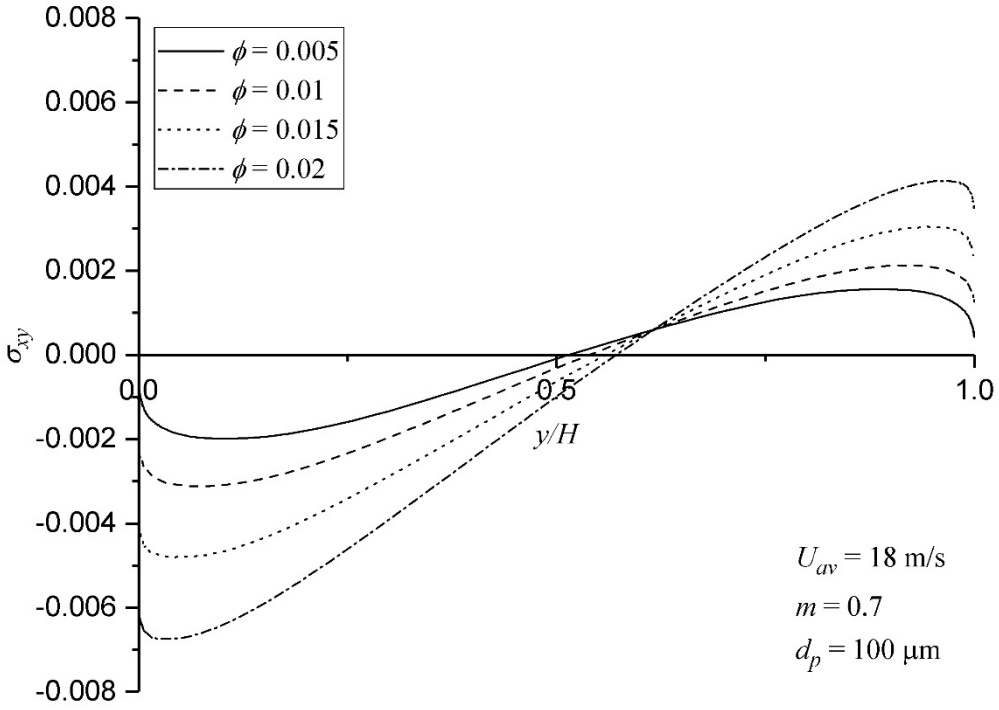

Figure 3.23: Solids shear stress predictions for different specularity coefficients

Table 3.5: Predicted peak and wall values for the solids shear stress

$\boldsymbol{\phi}$	$\boldsymbol{\sigma_{xy,peak-lower}}$	$\boldsymbol{\sigma_{xy,peak-upper}}$	$\boldsymbol{\tau_{w,lower}}$	$\boldsymbol{\tau_{w,upper}}$
0.005	0.00199	0.00159	0.0008	0.000431
0.01	0.00312	0.00213	0.00214	0.00126
0.015	0.0048	0.00305	0.00403	0.00225
0.02	0.00675	0.00413	0.00622	0.00352

In the current model, an increase in the specularity coefficient enhances the granular temperature. An elevated granular temperature indicates an increase in the particle-particle and particle-wall interactions which energizes the particle-phase. The elevated granular temperature also elevates the solids viscosity. The increase in solids viscosity enhances the solids shear stress. The asymmetry in the solids shear stress profiles arises due to asymmetry in the particle distribution across the channel, the asymmetry in the particle distribution is created by the gravity acting

transversely to the gas-solid flow in the channel. The increased solids viscosity results in a decrease in the solids velocity; the increasing asymmetry in the solids shear stress profiles results in a much weaker asymmetry in the solids velocity profiles.

3.3.2 Effect of Mass loading

Mass loading is a measure of the number of particles present at any given time in the gas-particle flow. So, the higher the mass loading, higher the number of particles in the flow. In the simulations, a particle size of d_p = 100 μm was considered and the bulk fluid velocity was maintained at U_{av} = 18 m/s, while the mass loading varied from from m = 0.4 to m = 1.0. The mass loading determines the bulk volume fraction of the particles. A mass loading m = 0.4 indicates a bulk volume fraction of α_{av} = 0.02%, while a mass loading of m = 1.0 indicates a bulk volume fraction of α_{av} = 0.05% (refer to Table 3.6), which implies that a dilute gas-solid flow was considered for the study. The specularity coefficient for the simulations was set at 0.005.

Figure 3.24 depicts the predictions for the solids velocity profile for various mass loadings. The solids velocity predictions show a minimal reduction, with a maximum difference of 0.5 % between the flows with a mass loading of m = 0.4 and m = 1.0. The solids velocity decreases slightly with the increase in mass loading, since the solids viscosity increases with an increase in the mass loading. The solids velocity profile is asymmetric, with a slightly higher velocity predicted at the upper wall than at the bottom wall. The solids shear stress (refer to Figure 3.29) is higher at the bottom wall than at the upper wall. A higher solids shear stress results in a lower solids velocity.

Figure 3.25 depicts the predictions for the normalized solids volume fraction profile. With an increase in mass loading, the particle concentration across the channel tends to homogenize, which is because of the increase in granular temperature (refer to Figure 3.26). Note that the bulk solids volume fraction increases with an increase in mass loading (see Table 3.6), which means an increased number of particles present in the flow. Asymmetry is observed in the solids volume fraction profiles with the solids volume fraction being higher at the bottom wall than at the top wall. This is due to the gravity acting in the transverse direction to the flow, which shifts the particles towards the bottom of the channel.

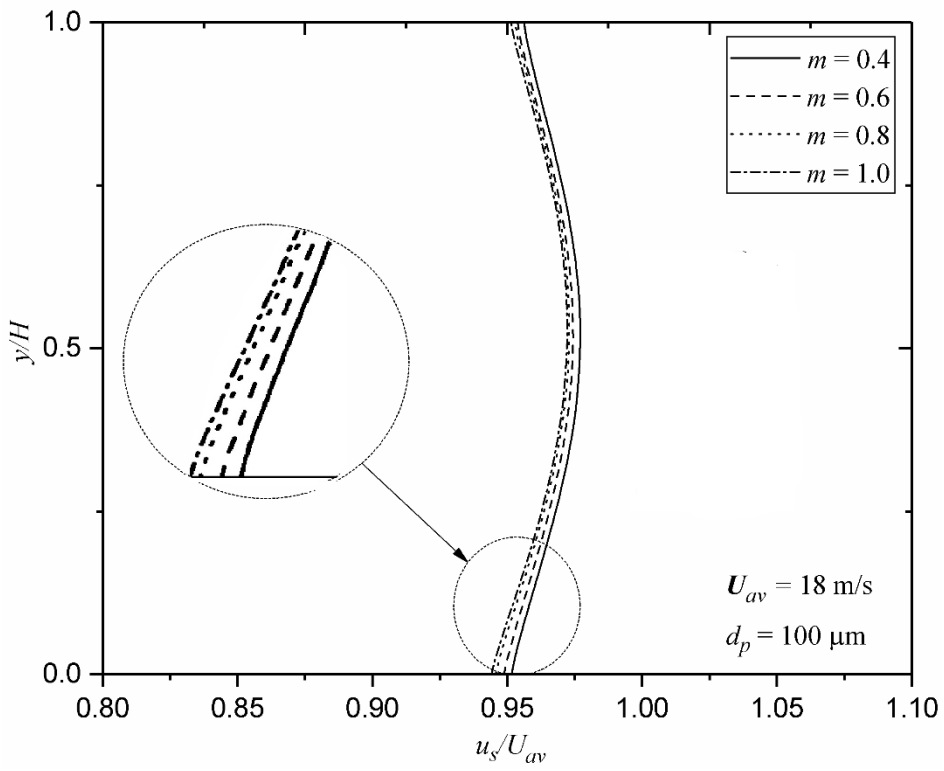

Figure 3.24: Solids velocity predictions for different mass loadings

Table 3.6: Bulk solids volume fraction for corresponding mass loading

m	α_{av} (%)
0.4	0.02
0.6	0.03
0.8	0.04
1.0	0.05

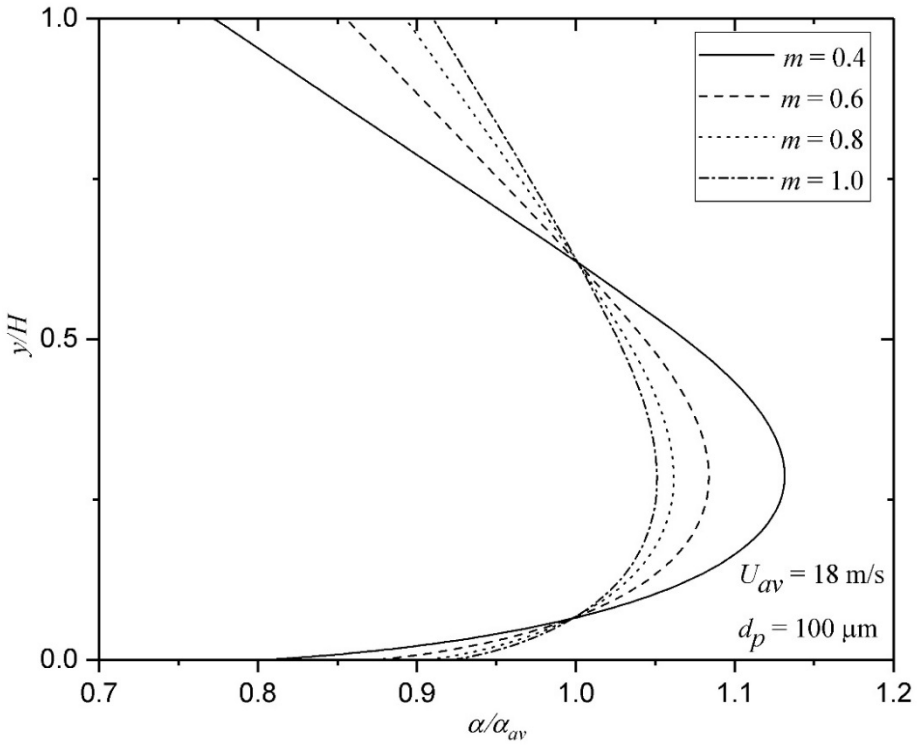

Figure 3.25: Solids volume fraction predictions for different mass loadings

Figure 3.26 depicts the predictions for the granular temperature. The level of the granular temperature increase with increases in mass loading. Recall that the bulk solids volume fraction increases with mass loading which means a higher frequency of particle-wall interactions which then results in a higher granular temperature. This may be due to the net production of granular temperature being maximum at the wall as a result of the particle-wall collisions. Since the turbulence kinetic energy peaks in the near-wall region, the turbulence modulation may also enhance the granular temperature in the near-wall region. Note that the granular temperature profiles are symmetric.

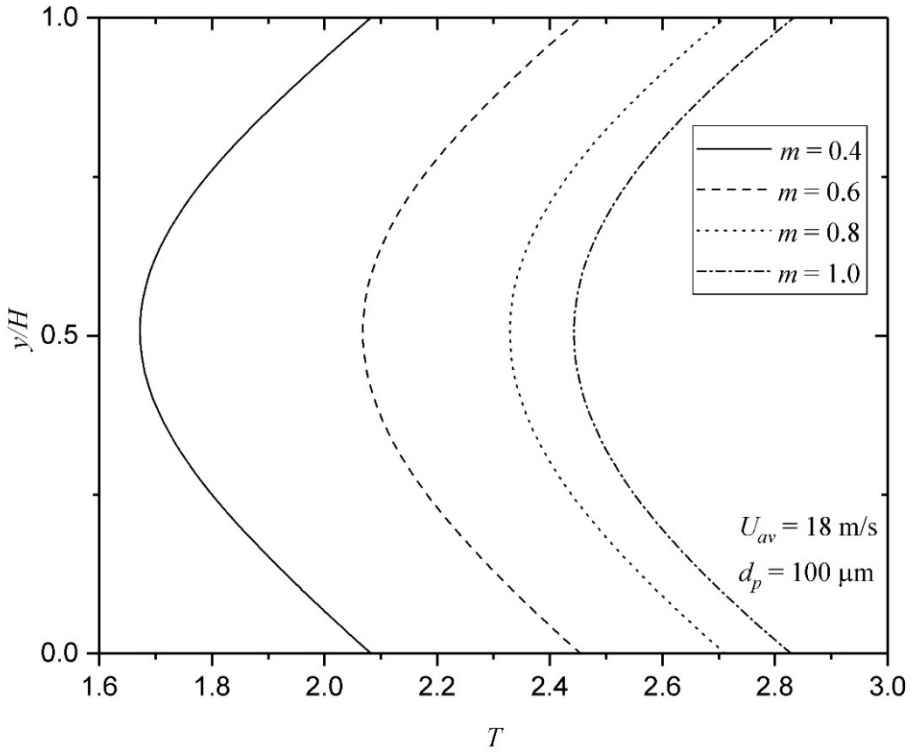

Figure 3.26: Granular temperature predictions for different mass loading

Figure 3.27 depicts the predictions for the corresponding solids viscosity. The solids viscosity increases with increase in mass loading. Mathematically, the solids viscosity is a function of the granular temperature, $\mu_s = \frac{5\sqrt{\pi}d_p\rho_s\sqrt{T}}{96}$, which implies that an increase in granular temperature increases the corresponding solids viscosity. The solids viscosity profiles are observed to peak at the top wall while a small off-wall peak is observed at the bottom wall.

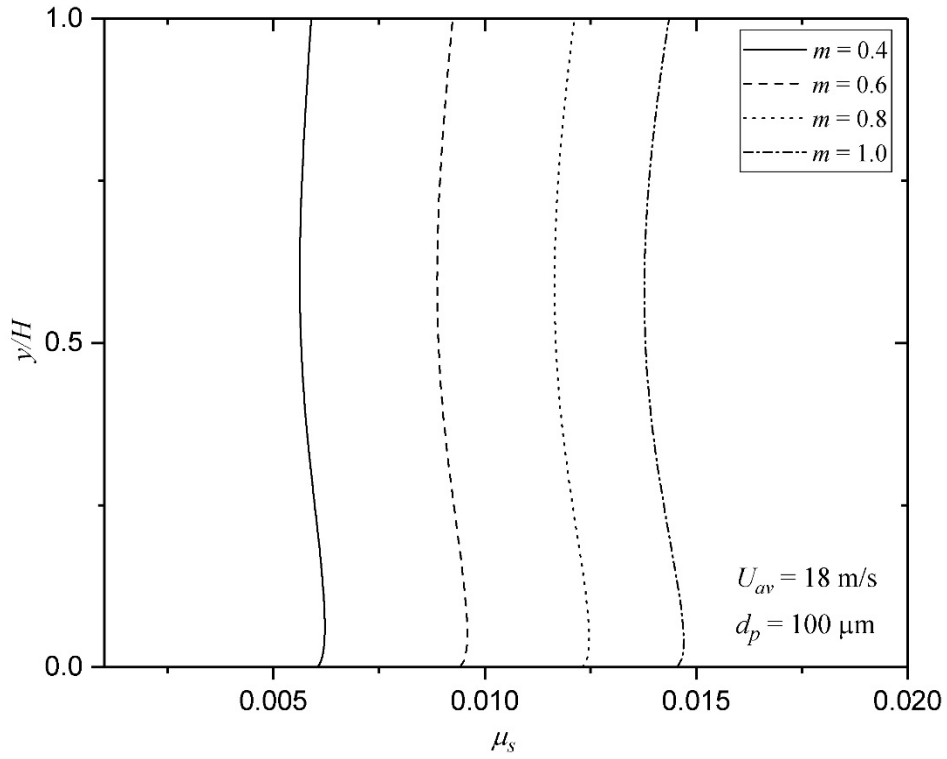

Figure 3.27: Solids viscosity predictions for different mass loadings

Figure 3.28 depicts the predictions for the solids shear stress for different mass loadings. Table 3.7 shows the corresponding solid shear stress values at the peaks and at the wall, both the peak and wall values increase with an increase in mass loading. Recall that an increase in mass loading increases the granular temperature, thus increasing the predicted solids shear stress. The distribution of shear stress is asymmetric: since the shear stress is closely coupled to the solids volume fraction, the asymmetry in the solids volume fraction results in a higher shear stress at the bottom wall and a lower shear stress at the upper wall. The asymmetry of the solids shear stress distribution across the channel increases with an increase in mass loading, which may be due to elevated granular temperature.

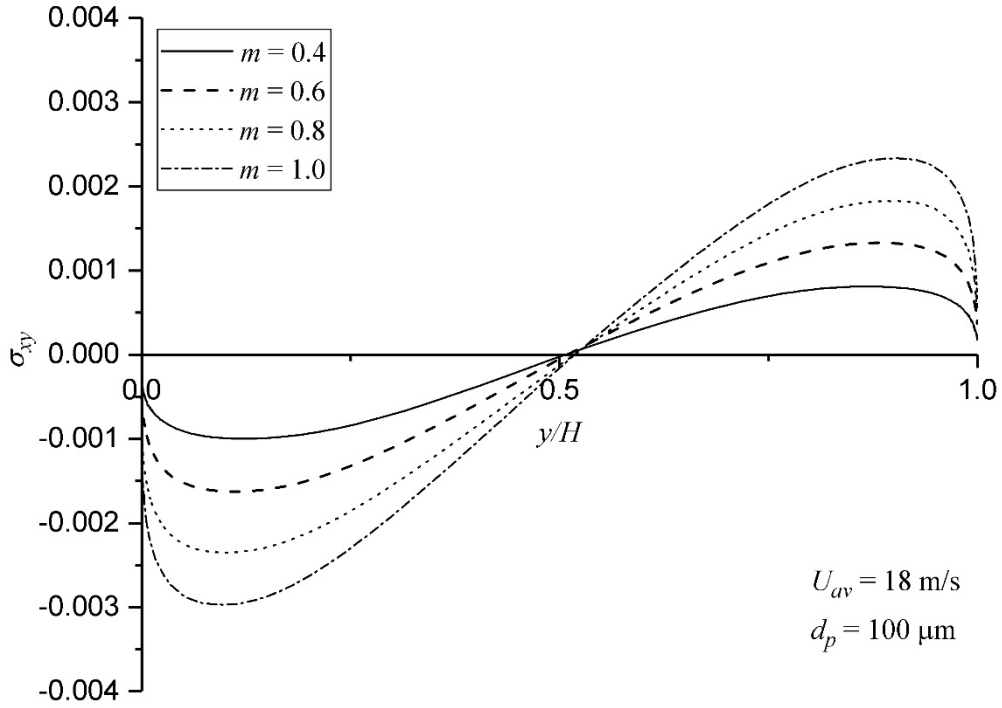

Figure 3.28: Solids shear stress predictions for different mass loadings

Table 3.7: Solids shear stress values for different mass loadings

m	$\sigma_{xy,peak-lower}$	$\sigma_{xy,peak-upper}$	$\tau_{w,lower}$	$\tau_{w,upper}$
0.4	0.001	0.00081	0.00031	0.00023
0.6	0.00162	0.00133	0.00062	0.00037
0.8	0.00235	0.00183	0.00092	0.00050
1.0	0.00297	0.00233	0.00123	0.00071

The current study indicates that an increase in mass loading marginally reduces the particle-phase velocity by elevating the solids viscosity. An increase in mass loading elevates the granular temperature by enhancing the frequency of particle-wall collisions. The elevated granular temperature also elevates the solids viscosity, as well as the solids shear stress. The solid-phase parameters are not affected by the nature of the particle-wall collisions determined using the

specularity coefficient. It is, however, affected by the frequency of the collisions which depends on the mass loading.

3.3.3 Effect of Stokes number

The Stokes number is the ratio of the particle response time to the characteristic time-scale of the flow and is a measure of the particle inertia. The Stokes number of the particle is determined using the relation,

$$St = \frac{d_p^2 \rho_s U_{av}}{18 \mu_f H} \tag{3.1}$$

As such the Stokes number *St* is a function of the particle diameter, the particle density, the bulk fluids velocity and the width of the channel. The Stokes number of the particle is defined using a time-scale based on the mean velocity of the fluid and the width of the channel. To study the effects of Stokes number on the flow, particle diameters of d_p = 100, 200, 500, and 1000 μm were considered for a particle of density ρ_s = 2500 kg/m^3. The Stokes number increases with an increase in particle diameter which leads to an increase in the particle response time. An intermediate particle mass loading of m = 0.7 and a bulk fluid-phase velocity of U_{av} = 18 m/s were selected, while the specularity coefficient was set to ϕ = 0.005.

Figure 3.29 depicts predictions for the solids velocity profile for particles with different Stokes numbers. The solids velocity monotonically decreases with an increase in the Stokes number. The reduction in solids velocity is due to the increase in solids viscosity (refer to Figure 3.33) with an increase in Stokes number. There is a gradual decrease in curvature of the profile with increasing Stokes number, which means that the solids velocity gradient also decreases.

Figure 3.30 depicts the normalized predictions for the solids volume fraction. Note that the solids volume fraction profiles for *St* = 95 and *St* = 595 appear to collapse. However, a more careful comparison of the dimensional profiles reveals small differences (refer to Figure 3.31). The value of solids volume fraction increases at the walls with Stokes number; the peak values decreases with an increase in the Stokes number. This is due to the increase in the granular temperature (refer to Figure 3.32). The increased granular temperature energizes the particle-phase, which as a result homogenizes across the channel. This implies that the particle distribution tends to homogenize with an increase in Stokes number.

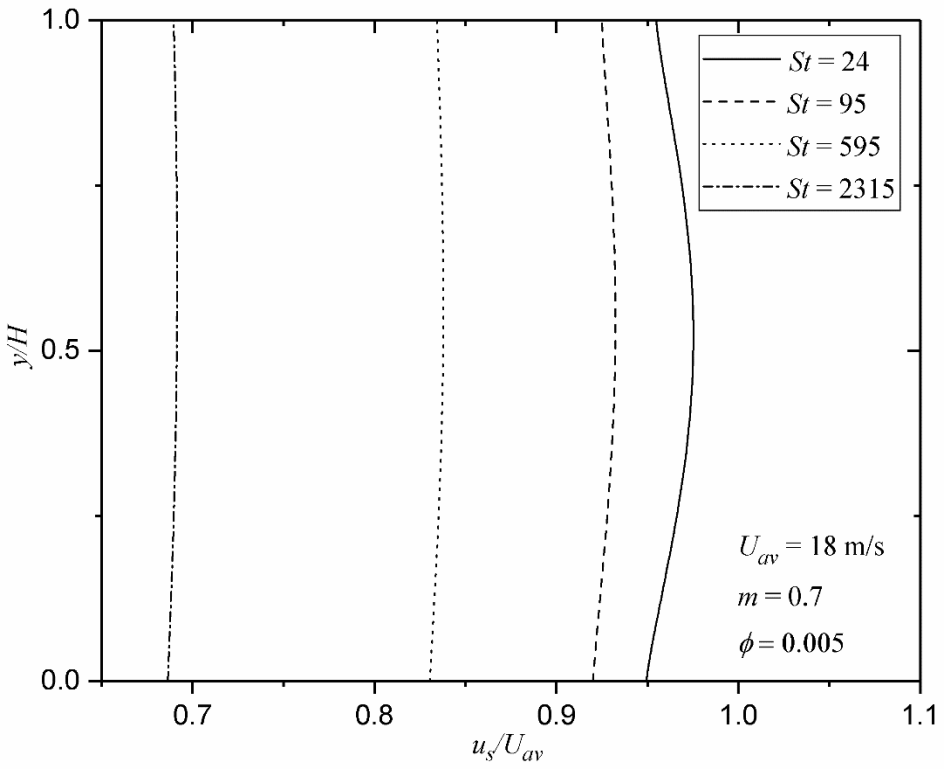

Figure 3.29: Solids velocity predictions for different Stokes numbers

Figure 3.31 depicts the non-normalized predictions for the solids volume fraction. The magnitude of the bulk solids volume fraction increases slightly with an increase in the Stokes number as seen in Table 3.8. The mass loading is kept constant for increasing the Stokes numbers. Note that the mass loading is defined as $m = \frac{\rho_s \sum \alpha_s u_s \Delta y}{\rho_f \sum (1-\alpha_s) u_f \Delta y}$, which implies that since the solids velocity decreases, to maintain the same mass loading, the bulk solids volume fraction is increased. These profiles indicate a small variation in shape as the Stokes number and the bulk solids volume fraction increases. However, the particle distribution for *St* = 2315 is more uniform that that for *St* = 595, which can be associated with the increase in the wake effect at higher Stokes numbers.

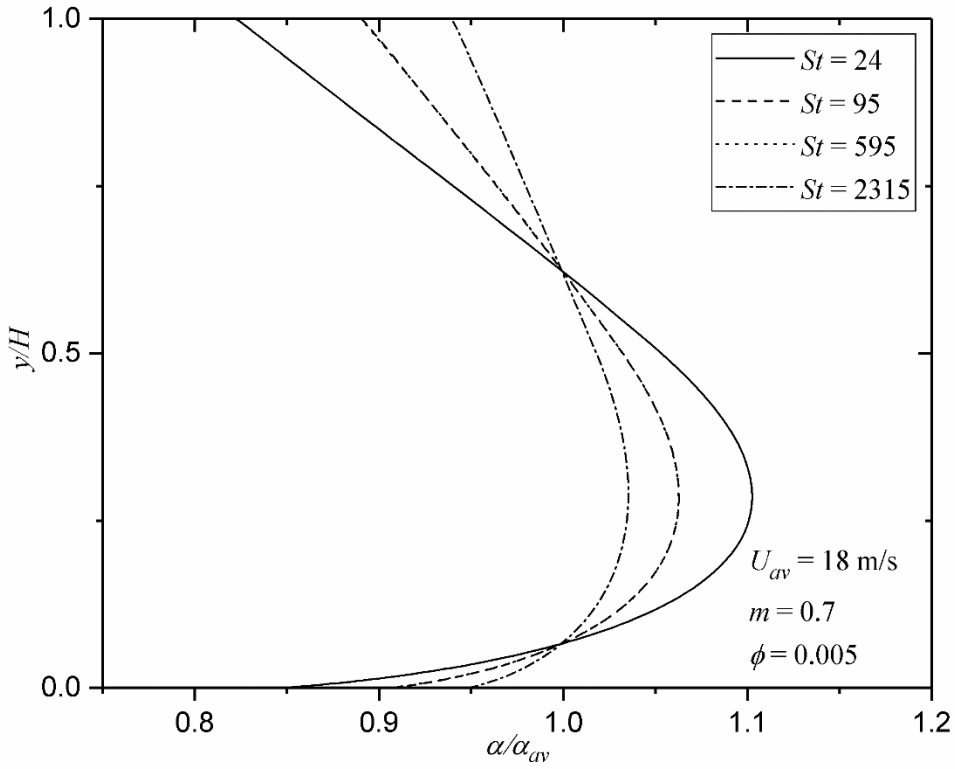

Figure 3.30: Normalized solids volume fraction predictions for different Stokes numbers

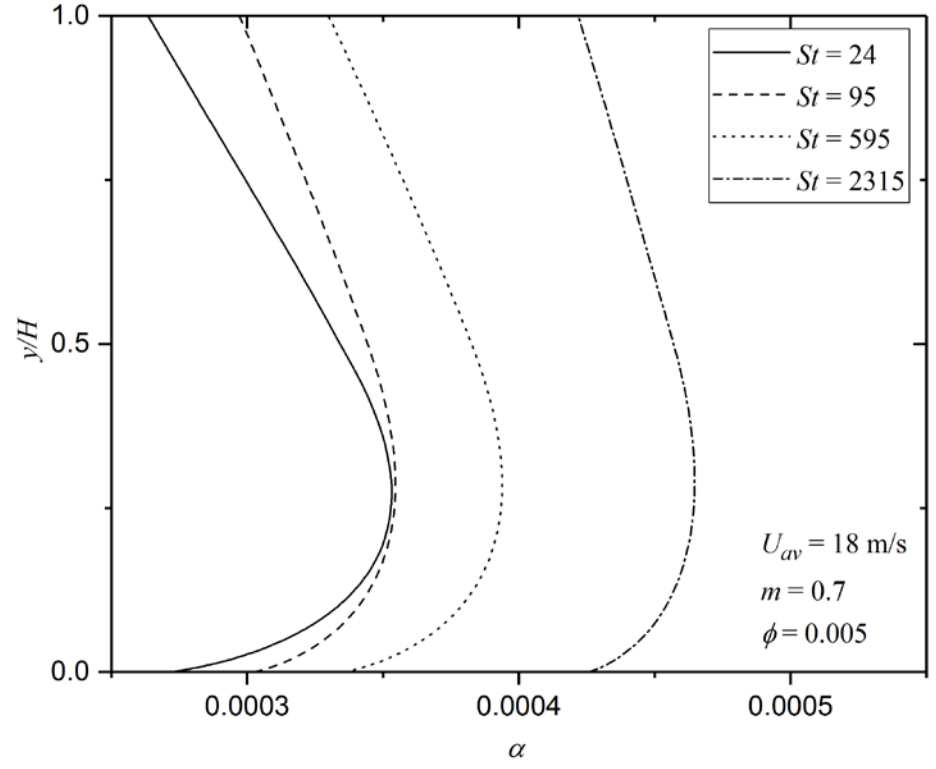

Figure 3.31: Solids volume fraction predictions for different Stokes numbers

Table 3.8: Bulk solids volume fraction for corresponding Stokes numbers

St	α_{av} (%)
24	0.035
95	0.036
595	0.039
2315	0.045

Figure 3.32 depicts the predictions for the granular temperature. The granular temperature levels do not exhibit a monotonic increase with an increase in Stokes number; the granular temperature at the center of the channel decreases by 12% between *St* = 95 and *St* = 595. The granular temperature profiles flatten with an increase in Stokes number. A change in curvature of the profile is also observed for the granular temperature profile for *St* = 2315; the granular temperature profile peaks at the center of the channel.

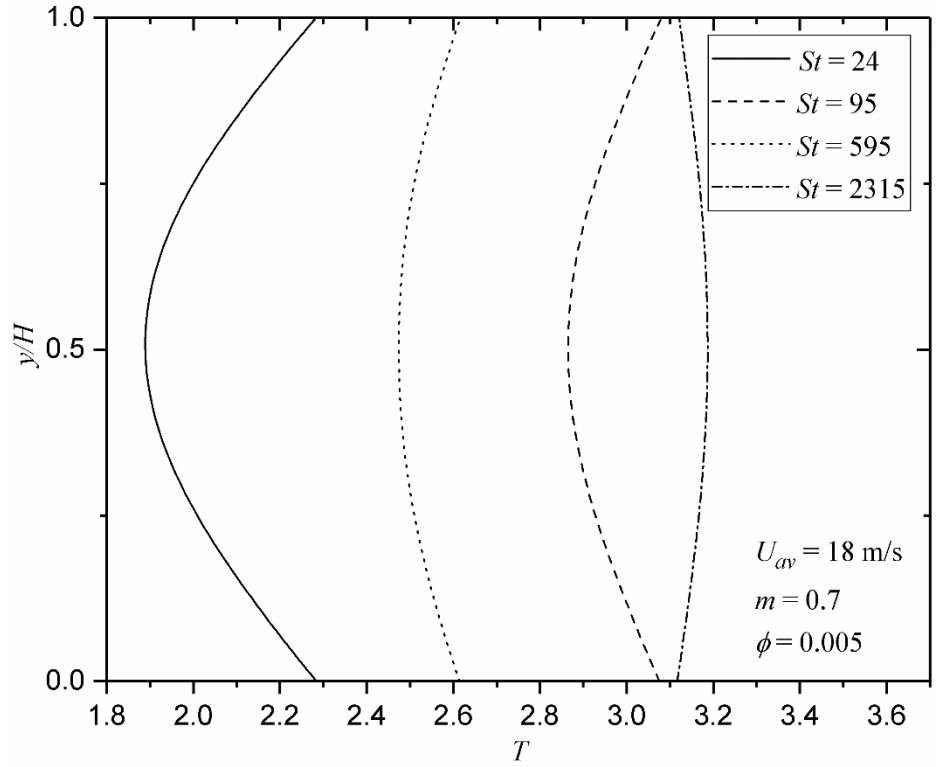

Figure 3.32: Granular temperature predictions for different Stokes numbers

Figure 3.33 depicts the predictions for the corresponding solids viscosity. The solids viscosity monotonically increases with an increase in the Stokes number. Mathematically, the solids viscosity is a function of the granular temperature and the particle diameter, $\mu_s = \frac{5\sqrt{\pi} d_p \rho_s \sqrt{T}}{96}$. Although the granular temperature does not increase in a monotonic fashion; the solids viscosity increases due to the increase in the particle diameter. This implies that the effect of particle diameter dominates over the effect of the granular temperature on the solids viscosity. The solids viscosity profiles flatten with an increase in the Stokes number. The profiles also exhibit a local extremum close to the bottom wall; for *St* = 24, 95 and 595 the extremum is a maxima, while for *St* = 2315 it is a minima. Since the granular temperature profile for *St* = 2315 changed its curvature, this results in a change in the curvature of the corresponding solids viscosity profile.

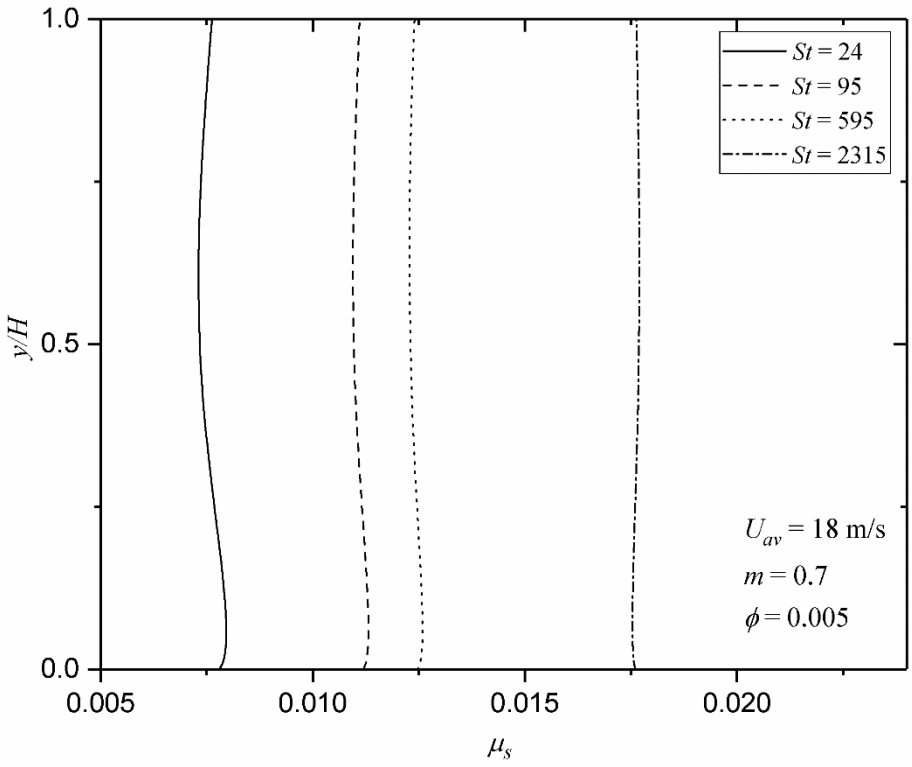

Figure 3.33: Solids viscosity predictions for different Stokes numbers

Figure 3.34 shows the solids shear stress predictions. The peak values of the solids shear stress is observed to decrease with an increase in the Stokes number. Mathematically, the solids shear stress is a function of the solids viscosity and the solids velocity gradient, i.e. $\sigma_{xy} = -\mu_s(\omega g_1 + g_2)\frac{\partial u_s}{\partial y}$. Since the solids velocity gradient decreases with an increase in the Stokes number, the solids shear

stress also reduces. This implies that the effect of the solids velocity gradient dominates over the effect of the solids viscosity on the solids shear stress. In addition to the decrease of the peak values of the solids shear stress, the location of the peak migrates towards the channel walls with an increase in Stokes number. The solids shear stress profiles are asymmetric due to the asymmetric solids volume fraction profile; an increase in the value of the solids volume fraction increases the value of the solids shear stress via the closure coefficients. The solids shear stress values at the walls are identical. Recall the specularity coefficient was kept constant at $\phi = 0.005$, which implies that the value of the specularity coefficient strongly affects the solids shear stress at the wall.

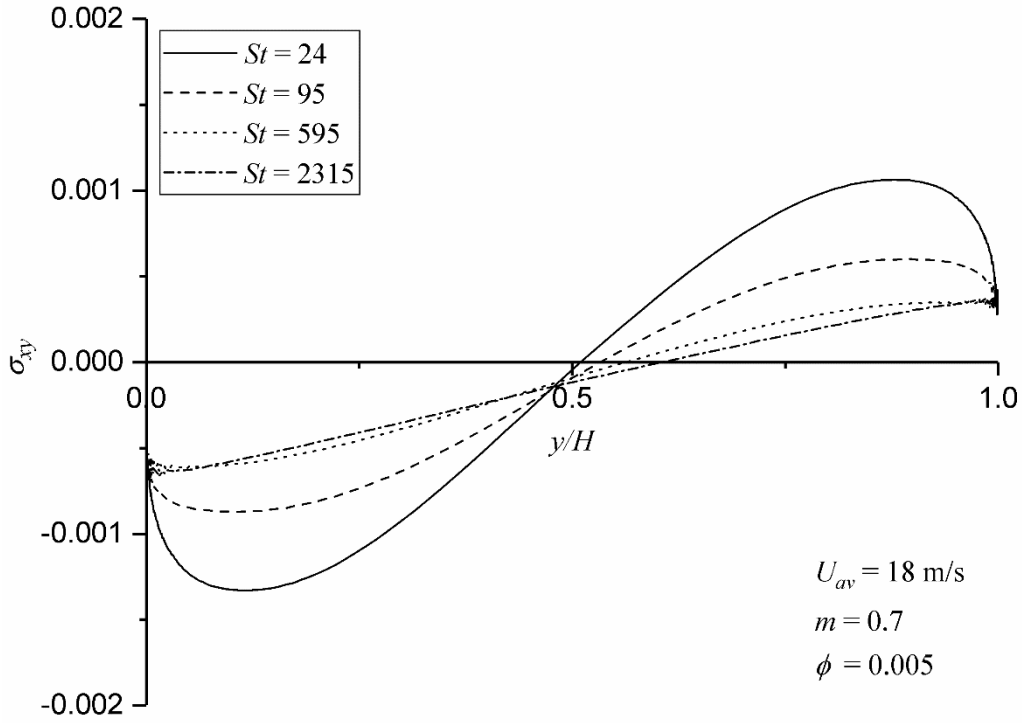

Figure 3.34: Solids shear stress for different Stokes numbers

The current study indicates that an increase in the Stokes number decreases the solids velocity. The solids volume fraction profiles indicate that the partilces tend to move towards the bottom of the channel between *St* = 95 and *St* = 595, while the profile for *St* = 2315 is more uniform, which may be due to the increasing wake effect, which increases with an increase in the particle diameter. The granular temperature does not decrease monotonously with an increase in the Stokes number; the granular temperature profile exhibits a change in curvature for the largest particle Stokes

number considered in the study. Small particles decrease the turbulence kinetic energy, which decreases the granular temperature via turbulence modulation; large particles increase the turbulence kinetic energy, which increases the granular temperature via turbulence modulation. The turbulence modulation near the center of the channel increases with an increase in the Stokes number (not shown), which is a result of the wake effect of the particles. The Stokes number St = 2315 results in a significant increase in the turbulence modulation near the center of the channel, which may partially explain the peak at the center of the channel in the corresponding granular temperature profile. The solids viscosity increases with an increase in Stokes number, which implies that the effect of particle diameter dominates the effect of granular temperature on the solids viscosity. The peak values for the solids shear stress decrease with an increase in Stokes number, which is due to the decrease in solids velocity gradient with an increase in Stokes number.

The study reveals the non-linear relation of the solids volume fraction and the granular temperature with Stokes number. In this context, the cause and/or mechanism for the change in curvature of the granular temperature and the solids viscosity profiles is not yet clear and warrants further study.

CHAPTER 4: SUMMARY AND CONCLUSIONS

The following chapter summarizes the conclusions and provides recommendations for future work based on the results of the simulations.

4.1 Summary of Simulations

The current dissertation explores the effects of wall roughness on the particle-phase properties of a turbulent gas-solid flow in a horizontal channel. An in-house numerical code was modified to simulate a fully developed turbulent gas-solid flow; the numerical code is based on the two-fluid formulation adopted from the model of Rao *et al.* (2011). The gas-solid flow in the horizontal channel is asymmetric due to the gravity acting transverse to the flow. Three different studies were conducted to document the response of the particle-phase properties to different flow conditions and parameters.

The first study focused on the effect of hydrodynamic roughness on the gas-solid flow. The hydrodynamic effect of wall roughness was implemented in the model using a two-layer version of the k - ε model. The simulation compared the flow for the rough wall with that for the smooth wall. Wall roughness alters the particle-wall interactions. The particle-wall interactions were characterized using the boundary conditions of Johnson and Jackson (1987), which introduced the specularity coefficient; this parameter was kept at the nominal value for a smooth wall in the first study.

The second study focused specifically on the role of the specularity coefficient in characterizing wall roughness; the channel wall was rough from a particle perspective but hydrodynamically smooth. The study matched the numerical and the experimental solids velocity profiles by calibrating the specularity coefficient. The outcomes of the simulations were compared to the experimental study of Sommerfeld and Kussin (2004). Their experiment explored the effect of different levels of wall roughness on the particle-phase properties; the wall roughness considered has negligible hydrodynamic contribution.

The third study focuses on the sensitivity of the particle-phase properties to three different parameters; the specularity coefficient, the mass loading and the Stokes number. The proportion of diffuse particle-wall collisions was increased by increasing the specularity coefficient; the effect on the particle-phase properties was documented. The increase in mass loading increased the number of particles present in the flow. The response of the particle-phase properties to the increase in mass loading was documented. The particle inertia was increased by increasing the Stokes number. The effect of increasing the particle response time to the flow on the particle-phase was explored.

4.2 Conclusions

Hydrodynamically rough flow conditions

The fluid-phase and the solid-phase in a gas-solid flow interact with each other via the particle drag term and the turbulence modulation term. The channel roughness introduces a hydrodynamic drag into the fluid phase, which reduces the fluid velocity near the wall, and enhances the turbulence kinetic energy and the Reynolds shear stress. The effect of roughness on the fluid-phase velocity is also reflected in the solids velocity through the drag term. The elevated granular temperature of the rough channel implies that the hydrodynamic roughness energizes the particles present in the flow through turbulence modulation. The volume fraction predictions for the rough channel show a more uniform distribution of particles, i.e. roughness tends to homogenize the particle distribution across the channel. The solids shear stress is also elevated due to turbulence modulation.

From the above observations, it can be concluded that hydrodynamic roughness tends to energize the particles present in the flow via the exchange of phasic fluctuations. A greater perspective would be obtained from experimental comparisons; however, no experimental studies that consider hydrodynamically rough conditions in a gas-solid channel flow were available.

Hydrodynamically smooth flow conditions

With the appropriate value of the specularity coefficient, the solid-phase mean velocity profiles were found to be within 5% of the experimental data, the degree of deviation reduced with an increase in the roughness. The solids volume fraction predictions deviated most in the near-wall regions from the available data, either over-predicting or under-predicting the experimental data. Again, the degree of deviation decreased with an increase in the roughness. An increase in

roughness makes the particle distribution across the channel more uniform due to the elevated granular temperature. The increase in granular temperature energizes the particles present. The energized particles also elevate the solids viscosity predictions, as well as the solids shear stress predictions with increasing levels of roughness. An enhanced solids viscosity results in a greater resistance to particle flow which decreases the solids velocity for increased roughness.

It can be concluded that the specularity coefficient plays a significant role in characterizing channel wall roughness. However, the specularity coefficient is less effective for the walls with smaller roughness.

Sensitivity analysis

An increase in the specularity coefficient elevated the granular temperature. The elevated granular temperature also elevated the solids viscosity. The increased solids viscosity enhanced the solids shear stress. The increased solids viscosity results in the decrease of the solids velocity; the increasing asymmetry in the solids shear stress profiles marginally increases the asymmetry in the solids velocity profiles. It can be concluded that under identical flow conditions, the specularity coefficient significantly affects the particle-phase property variation across the channel. The specularity coefficient is a controlling parameter for the particle properties at the wall, i.e. granular temperature and solids shear stress.

An increase in mass loading marginally reduces the particle-phase velocity by elevating the solids viscosity. An increase in mass loading elevates the granular temperature by enhancing the frequency of particle-wall collisions. The elevated granular temperature also elevates the solids viscosity, as well as the solids shear stress. It can be concluded that the particle-phase properties are affected by the frequency of the collisions which depends on the mass loading.

An increase in the Stokes number decreases the solids velocity. The granular temperature decreases, but not monotonically, with an increase in Stokes number; the granular temperature profile exhibits a change in curvature for the largest Stokes number considered in the study. The solids viscosity increases with an increase in Stokes number, which implies that the effect of particle diameter dominates the effect of granular temperature on the solids viscosity; the solids viscosity profile changes curvature, albeit the curvature is minimal, for high Stokes number values. It can be concluded that the relationship between the Stokes number and particle-phase properties

such as granular temperature, solids viscosity and solids volume fraction is highly non-linear. The lack of an identifiable cause and/or mechanism for the relationship warrants further investigation.

4.3 Future work

The current study of numerically simulating turbulent gas-solid flows has identified the following issues which warrant further study:

1) The current dissertation presents two different studies that separately focus on the effect of hydrodynamic roughness and wall roughness on the particle-phase properties. The next step would be to combine the two aspects of roughness into a single study. However, such a study also requires a corresponding set of experiments that consider hydrodynamically rough conditions in a gas-solid channel flow.
2) The current mathematical model adopts the boundary condition of Johnson and Jackson (1987) and uses the specularity coefficient to implement the effect of roughness on the particles. The boundary condition was found to be less effective for walls with lower roughness. It would be of interest to implement a wall boundary condition for the particle-phase based on the model of Soleimani *et al.* (2015) and assess the performance.
3) The current mathematical model uses a single equation closure model for the solid-phase granular temperature in which the dissipation is expressed as a simple algebraic relation. It would be of interest to introduce a set of transport equations for the turbulent particle fluctuations such as the $k_p - \varepsilon_p$ model of O'Brien (2014).
4) Although the wake term model used by Rao *et al.* (2011), correctly predicts the turbulence enhancement due to large particles, the expression is crude and requires refinement to produce more accurate predictions that can be used to define regimes for gas - solid flows based on the Stokes number.
5) The cross correlation term of Sinclair and Mallo (1998) fails to capture the turbulence modulation in the near-wall region. It would be of interest to explore and implement alternative cross-correlation terms to improve the near-wall behavior of the model.
6) Due to the diffuse nature of particle-wall collisions at the rough wall, it would be of interest to explore the flow in a 3D and unsteady Lagrangian framework.

REFERENCES

Batchelor, G. & Green, J., 1972. The determination of bulk stress in a suspension of spherical particle. *Journal of Fluid Mechanics,* Volume 56, pp. 401 - 427.

Benyahia , S., Syamlal, M. & O'Brien, T., 2007. Study if the ability of multiphase continuum models to predict core-annulus flow. *AIChe J.,* Volume 53, pp. 2549-2568.

Bolio, E. J. & Sinclair, J. L., 1995. Gas turbulence modulation in the pneumatic conveying of massive particles in vertical tubes. *Int. J. Multiphase Flow,* 21(6), pp. 985-1001.

Bolio, E., Yasuna, J. & Sinclair, J., 1995. Dilute turbulent gas-solid flow in risers with particle-particle interactions. *AIChe Journal,* Volume 41, pp. 1375-1388.

Bolio, E., Yasuna, J. & Sinclair, J., 1995. Dilute turbulent gas-solid flow in risers with particle-particle interactions. *AIChe J.,* Volume 41, pp. 1375-1388.

Cao, J. & Ahmadi, G., 2000. Gas-particle two-phase turbulent flow in horizontal and inclined ducts. *Int. J. Engineering Science,* 38(17), pp. 1961-1981.

Chen, C. J. & Patel, V. C., 1988. Near-wall turbulence models for complex flows including separation. *AIAA J.,* Volume 26, pp. 1375-1388.

Crowe, C. T., 2000. On models for turbulence modulation in fluid-particle flows. *Int J. Multiphase Flow,* Volume 26, pp. 710-727.

Ding, J. & Gidaspow, D., 1990. A bubbling fluidization model using kinetic theory of granular flow. *AIChe J.,* 36(4), pp. 523-538.

Durbin, P. A. *et al.,* 2001. Rough wall modification of two-layer k – ε. *J. Fluids Engg.,* Volume 123, pp. 16-21.

Fox, R., 2014. On multiphase turbulence models for collisional fluid-particle flows. *J. Fluid Mech.,* Volume 742, pp. 368-424.

Gore, R. & Crowe, C., 1989. Effect of particle size on modulating turbulent intensity. *Int. J. Multiphase Flow,* Volume 15, pp. 279-285.

Hadinoto, K. & Curtis, J., 2009. Numerical simulation of turbulent particle laden flow with significant fluid to particle inertia ratio. *Ind. Eng. Chem. Res.,* Volume 48, pp. 5874-5884.

Hill, R., Koch, D. & Ladd, J., 2001-a. The first effects of fluid inertia on flows in ordered and random arrays of spheres. *J. Fluid Mech.,* Volume 448, pp. 213-241.

Hill, R., Koch, D. & Ladd, J., 2001-b. Moderate Reynolds number flows in ordered and random arrays of spheres. *J. Fluid Mech.,* Volume 448, pp. 243-278.

Ishii, M. & Hibiki, T., 2006. *Thermo-fluid Dynamics of Two-Phase flow.* 2nd ed. New York: Springer.

Johnson, P. C. & Jackson, R., 1987. Frictional-collisional constitutive relations for granular materials. *Journal of Fluid Mechanics,* Volume 176, pp. 67-94.

Koch, D., 1990. Kinetic theory for a monodisperse gas-solid suspension. *Phys. Fluid. A,* Volume 2, pp. 1711-1723.

Kussin, J. & Sommerfeld, M., 2002. Experimental studies on particle behaviour and turbulence modification in horizontal channel flow with different wall roughness. *Experiments in Fluids,* 33(1), pp. 143-159.

Louge, M., Mastorakos, E. & Jenkins, J., 1991. The role of particle collisions in pneumatic transport. *J. Fluid Mech.,* Volume 231, pp. 345-359.

Lun, C., Savage, S., Jeffery, D. & Chepurniy, N., 1984. Kinetic theories for granular flow: inelastic particles in couette flow and slightly inelastic particles in a general flow field. *J. Fluid. Mech.,* Volume 140, pp. 223-256.

Myong, H. K. & Kasagi, N., 1990. A new approach to the improvement of turbulence model for wall-bounded shear flows. *JSME Int. J. (II),* 33(1), pp. 63-72.

O'Brien, T., 2014. A multiphase turbulence theory for gas-solid flows: I. Continuity and momentum equations with Favre-averaging. *Powder Technol.,* Volume 2014, pp. 83-87.

Owen, R. G., Hunt, J. & Collier, J. G., 1976. Magnetohydrodynamic pressure drop in ducted two-phase flows. *Int. J. Multiphase Flow,* Volume 3, pp. 23-33.

Patankar, S. V., 1980. *Numerical Heat Transfer and Fluid Flow.* 1st ed. New York: Hemishpere Publishing Corp. .

Peirano, E. & Leckner, B., 1998. Fundamentals of turbulent gas-solid applied to circulating fluidized bed combustion. *Progr. Energy Combut. Sci.,* Volume 24, pp. 259-296.

Rao, A., Curtis, J. S., Hancock, B. B. & Wassgren, C., 2011. Numerical simulation of dilute turbulent particle flow with turbulence modulation. *AIChe J.,* 58(5), pp. 1381-1396.

Schneiderbauer, S., Schellander, D., Loderer, A. & Pirker, S., 2012. Non-steady state boundary conditions for collisional granular flows at flat frictional moving walls. *Int. J. Multiphase flows,* Volume 43, pp. 149-156.

Sinclair, J. & Jackson, R., 1989. Gas-particle flow in a verticla pipe with particle-particle interactions. *AIChe J.,* Volume 35, pp. 1473-1486.

Sinclair, J. L. & Mallo, T., 1998. *Describing particle-turbulence interaction in a two-fluid modeling framework.* Washington, D C, Proc. of ASME Fluids Engineering Division Summer Meeting (FEDSM'98).

Soleimani, A., Pirker, S. & Schneiderbauer, S., 2015. Solid boundary condition for collisional gas–solid flows at rough walls. *Powder Technology,* Volume 281, pp. 28-33.

Sommerfeld, M. & Huber, N., 1999. Experimental analysis and modelling of particle-wall collisions. *Int. J. of Multiphase Flow,* Volume 25, pp. 1457-1489.

Sommerfeld, M. & Kussin, J., 2004. Wall roughness effects on pneumatic conveying of spherical particles in a narrow horizontal channel. *Powder Technology,* Volume 142, pp. 180-192.

Wen, C. & Yu, Y., 1966. Mechanics of fluidization. *Chem. Eng. Porgr. Symp. Ser.,* Volume 62, pp. 100-111.

Yeh, Y. & Cummins, H. Z., 1964. Localized Fluid Flow Measurements with He-Ne Laser Spectrometer. *Applied Physics Letter,* 4(10), pp. 176-178.

Yerrumshetty, A. K., 2007. *Numerical prediction of turbulent gas-sold and liquid-solid flows using two-fluid models,* Saskatoon: University of Saskatchewan .

Yuan, Z. & Michaelides, E. E., 1992. Turbulence modulation in particle flows - A theoretical approach. *Int. J. Multiphase Flow*, 18(5), pp. 779-785.

Zaman, A. U., 2013. *Numerical analysis of turbulent gas-solid flows in a vertical pipe using the Eulerian tow-fluid model*, Saskatoon: University of Saskatchewan.

Zaman, A. U. & Bergstrom, D. J., 2014. Implementation of Two-Fluid Model for Dilute Gas-Solid Flow in Pipes with Rough Walls. *Journal of Fluids Engg*, Volume 136, pp. 031301-1-11.

Zhang, Y. & Reese, J. M., 2001. Particle-gas turbulence interactions in a kinetic theory approach to granular flows. *Int. J. Multiphase Flow*, Volume 27, pp. 1945-1964.

Zhang, Y. & Reese, J. M., 2003. Gas turbulence modulation in a two-fluid model for gas-solid flows. *AIChe J.*, 49(12), pp. 3048-3065.